72-18

GEOLOGICAL SURVEY OF CANADA

DEPARTMENT OF ENERGY, MINES AND RESOURCES

PAPER 72-18.

COMPACTION AND FLUID MIGRATION IN CRETACEOUS SHALES OF WESTERN CANADA

(Report and 46 figures)

K. Magara

Price, $3.00

1973

CANADA

GEOLOGICAL SURVEY OF CANADA

PAPER 72-18

COMPACTION AND FLUID MIGRATION IN CRETACEOUS SHALES OF WESTERN CANADA

K. Magara

DEPARTMENT OF ENERGY, MINES AND RESOURCES

Available by mail from *Information Canada*, Ottawa

from the Geological Survey of Canada
601 Booth St., Ottawa

and

Information Canada bookshops in

HALIFAX - 1687 Barrington Street
MONTREAL - 640 St. Catherine Street West
OTTAWA - 171 Slater Street
TORONTO - 221 Yonge Street
WINNIPEG 393 Portage Avenue
VANCOUVER - 680 Robson Street

or through your bookseller

Price: $3.00 Catalogue No. M44-72-18

Price subject to change without notice

Information Canada
Ottawa
1973

CONTENTS

Page

Illustrations

Page

Page

ABSTRACT

Shale porosity distributions within Cretaceous and Tertiary rocks of the Alberta and Saskatchewan subsurface have been determined by the use of sonic and formation density logs, and the examination of cores and surface rock samples. At shallow depths, shale porosity appears to be related exponentially to depth. Porosity at depth in Cretaceous shales, especially in the western part of the area studied, tends to be greater than the porosity-depth trend established at shallower depths would suggest, and is associated with anomalously high fluid pressure conditions.

Fluid pressure gradients in shales can be determined by the porosity distribution, as derived from sonic logs, of incompletely compacted shales. Differing permeabilities in shales may be estimated through use of the fluid pressure gradient and Darcy's law. Calculated shale permeabilities and porosity values can then be integrated to establish a subsurface interrelationship. This method of analysis, applied to Cretaceous shales in the subsurface of Alberta and Saskatchewan, reveals that the permeability increases less with increase in porosity than the amount given by Archie's relation, which is based on sandstone and carbonate rocks. This calculated porosity-permeability relationship for shales has been verified in numerous other studies by laboratory-measured porosity and permeability data.

Anomalously high pressures in the deep subsurface can be explained by fluid expulsion mechanisms related to compaction of shales. The volume of fluids which should be expelled from shales in unit time to reach compaction equilibrium may be determined for several different rates of sedimentation, based on the shale porosity data in western Canada. For each rate of sedimentation or subsidence there is a minimum permeability for reaching compaction equilibrium, which may be calculated according to Darcy's law. Comparison of this calculated minimum permeability with actual shale permeabilities, determined by laboratory measurements, suggests that, at relatively shallow depths, shale usually should be permeable enough to permit the attainment of compaction equilibrium and to maintain normal hydrostatic pressure. At depth, however, actual permeabilities are less than the calculated minimum necessary for compaction equilibrium, so that abnormal pressures may occur; the incidence of such abnormal pressures should increase with increases in the rate of sedimentation and in the total thickness of the sequence.

Shale porosity distribution in incompletely compacted shale zones also may be affected by the permeability and the extent of adjacent sandstone or carbonate rock bodies. A sharp decrease of porosity in shales close to such rock bodies would suggest that relatively large volumes of fluids have been expelled from the shales into the adjacent sandstones or carbonates. If this expelled fluid volume is large, the possibility of hydrocarbon accumulation in such sandstone or carbonate rocks is considered to be favorable. To illustrate such a study, Cretaceous shales associated with hydrocarbon reservoirs in the subsurface of northwestern Alberta and northeastern British Columbia have been examined. Most Mesozoic oil and gas pools in this area are concentrated where a large volume of fluids is considered to have been expelled downward from the overlying shales.

To obtain laboratory data on compaction and fluid expulsion relationships, a number of experiments were conducted on several kinds of clays. The results yielded porosity distributions similar to those of Cretaceous shales in the subsurface of western Canada.

RÉSUMÉ

Les répartitions de la porosité du schiste argileux dans les roches du Crétacé et du Tertiaire du sous-sol de l'Alberta et de la Saskatchewan ont été déterminées au moyen de diagrammes soniques et de densité des couches, de l'examen de carottes et d'échantillons de roches de surface. A de faibles profondeurs, la porosité du schiste argileux semble exponentiellement reliée à la profondeur. La porosité en profondeur dans les schistes argileux du Crétacé, particulièrement dans la partie ouest de la région étudiée, tend à devenir plus importante que la courbe porosité-profondeur trouvée à de faibles profondeurs ne le laisserait supposer, et elle est associée à des conditions de pression des fluides anormalement élevée.

Les gradients de pression des fluides dans les schistes argileux peuvent être déterminés par la répartition de la porosité, telle que dérivée des diagrammes soniques, des schistes argileux incomplètement compactés. Les perméabilités différentes dans les schistes argileux peuvent être évaluées au moyen du gradient de pression des fluides et de la loi de Darcy. Les valeurs calculées des perméabilités et de la porosité du schiste argileux peuvent être intégrées pour établir une corrélation souterraine. Cette méthode d'analyse, appliquée aux schistes argileux du Crétacé dans le sous-sol de l'Alberta et de la Saskatchewan, révèle que la perméabilité augmente moins avec l'accroissement de la porosité que la somme donnée par la relation d'Archie, laquelle est basée sur le grès et les roches carbonatées. Cette relation calculée de la porosité en fonction de la perméabilité s'est vérifiée dans de nombreuses études sur des données de porosité et de perméabilité mesurées en laboratoire.

Les pressions anormalement élevées dans le sous-sol profond peuvent s'expliquer par des mécanismes d'expulsion des fluides reliés à la compaction des schistes. Le volume des fluides qui pourrait être expulsé des schistes

argileux par unité de temps pour atteindre l'équilibre de compaction peut être déterminé pour plusieurs différents taux de sédimentation, en se basant sur les données de porosité du schiste argileux de l'Ouest canadien. Pour chaque taux de sédimentation ou de subsidence, il existe une permabilité minimum permettant l'équilibre de compaction, qui peut être calculée selon la loi de Darcy. La comparaison de cette perméabilité calculée avec les perméabilités réelles du schiste argileux, déterminées par des mesures effectuées en laboratoire, laisse entrevoir qu'à des profondeurs relativement faibles, le schiste argileux serait ordinairement assez perméable pour permettre d'atteindre l'équilibre de compaction et de garder une pression hydrostatique normale. En profondeur, toutefois, les perméabilités réelles sont inférieures au minimum calculé nécessaire à l'équilibre de compaction, ce qui peut être la cause de pressions anormales; le nombre de ces phénomènes de pressions anormales s'accroîtrait en fonction de l'augmentation du taux de sédimentation et de l'épaisseur totale de la série.

La répartition de la porosité du schiste argileux dans des zones de schiste argileux incomplètement compactées peut aussi être influencée par la perméabilité et l'étendue des massifs adjacents de grès ou de roches carbonatées. Une diminution rapide de la porosité des schistes argileux situés près de ces massifs rocheux pourrait signifier que des volumes de fluide relativement importants ont été expulsés des schistes argileux dans les grès et les roches carbonatées adjacents. Si le volume de fluide expulsé est important, il est possible que des hydrocarbures se soient accumulés dans ces grès et ces roches carbonatées. Pour illustrer cette étude, des schistes argileux du Crétacé associés à des réservoirs d'hydrocarbures dans le sous-sol du nord-ouest de l'Alberta et du nord-est de la Colombie-Britannique ont été examinés. La plupart des gisements de pétrole et de gaz du Mésozoïque de cette région sont concentrés aux endroits où on croit que d'importants volumes de fluide ont été expulsés vers le bas à partir des schistes argileux sus-jacents.

Pour obtenir des données en laboratoire sur les relations entre la compaction et l'expulsion des fluides, des expériences ont été effectuées sur plusieurs sortes d'argiles. Les résultats ont donné des répartitions de porosité semblables à celles des schistes argileux du Crétacé du sous-sol de l'Ouest du Canada.

COMPACTION AND FLUID MIGRATION IN CRETACEOUS SHALES OF WESTERN CANADA

INTRODUCTION

As part of a study of compaction and fluid migration in Cretaceous and Tertiary rocks of the central and western Interior Plains of Canada, shale porosity distribution and fluid pressure gradients have been determined by means of sonic and formation density logs and by visual examination of subsurface rock samples. Regions of anomalously high fluid pressure are recognized in Cretaceous shales, especially in the western part of the area, and can be explained by fluid expulsion mechanisms related to compaction. The sharp decrease of porosity in shale close to sandstone or carbonate bodies would suggest that relatively large volumes of fluid have been expelled from the shales into them and that the possibility of hydrocarbon accumulation may be enhanced. Interestingly enough, most Mesozoic oil and gas pools in northwestern Alberta and northeastern British Columbia are concentrated where a large volume of fluids is considered to have been expelled.

The evaluation of the phenomenon of compaction and fluid migration in the search for potential hydrocarbon reservoirs will be dealt with under six headings: shale porosity distribution, porosity-permeability relationships of shale, causes of abnormal pressures, amount of fluids expelled, compaction experiments using clays, and trends of future research.

Acknowledgments

The work covered by this report was carried out between August 1967 and 1969 at the Institute of Sedimentary and Petroleum Geology of the Geological Survey of Canada in Calgary, Alberta. The project was supported by a Post-doctorate Fellowship from the National Research Council. The author wishes to

---

Original Manuscript submitted: December 10, 1970.
Final version approved for publication: April 11, 1972.
Author's address: Imperial Oil Enterprises, Calgary, Alberta.

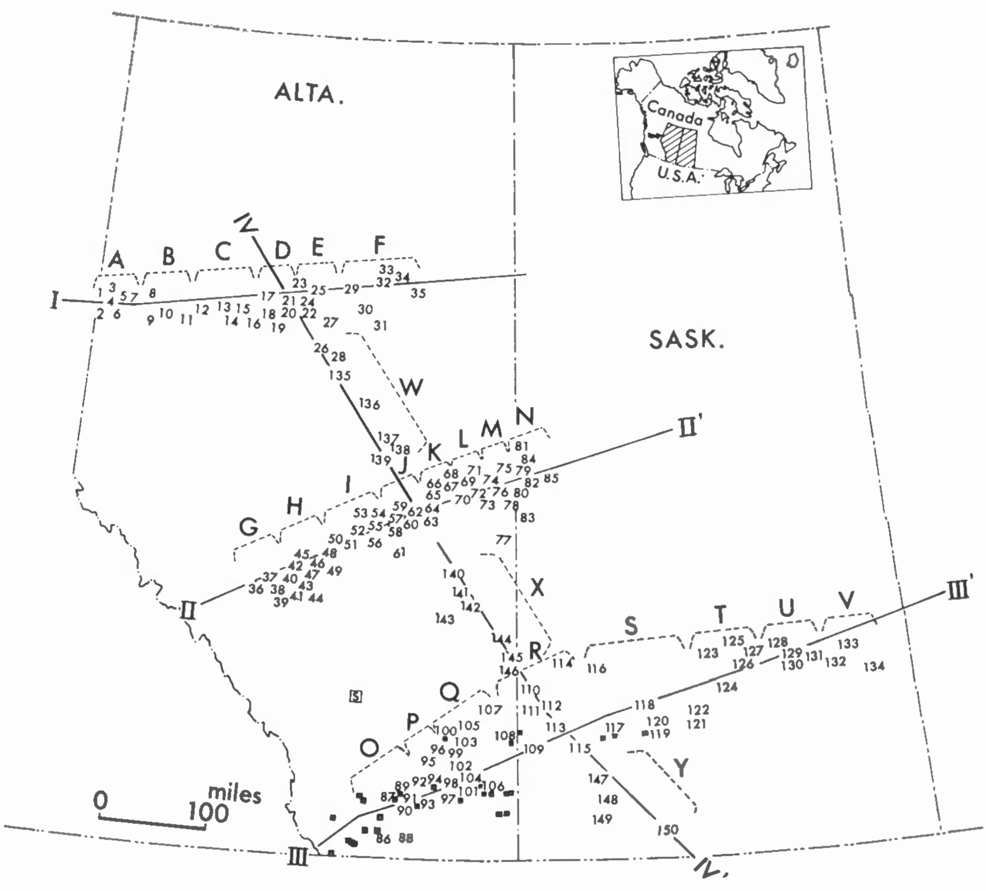

Wells studied 148

Groups of wells .... E

Location showing surface shale samples .... ■

Location of Strathmore well 7-12-25-25-W4 .... [S]

Figure 1. Index map showing location of wells studied (Appendix, Table I)

express his appreciation for the advice and supervision provided by Dr. D.J. McLaren, Director of the Institute, and Dr. D.K. Norris, head of the Structural Geology Section. Drs. R.G. McCrossan, R.W. Macqueen, C.J. Yorath and R.M. Procter, also of the Institute, provided research assistance and helpful comment, as did Dr. Brian Hitchon of the Research Council of Alberta in Edmonton. Mr. G.M. Peterkin of the Institute constructed the apparatus for the compaction experiments. Miss J.B. Greig of Imperial Oil Limited contributed editorial advice.

RELATIONSHIPS BETWEEN SHALE POROSITY, FLUID PRESSURE AND DEPTH

More than 160 wells, all with sonic logs, have been studied in the subsurface of Alberta and Saskatchewan (Fig. 1). In 14 of these wells, both sonic and formation density logs have been run (Table 1). Because the formation density log provides both density and porosity values, the relationship between porosity and acoustic transit time can be determined by using data from both logs.

After numerous laboratory tests, Wyllie *et al.* (1956, 1958) concluded that, in consolidated strata with uniformly distributed small pores, there is a linear relationship between porosity and transit time:

$$\Delta t_{log} = \phi \cdot \Delta t_{liquid} + (1 - \phi)\ \Delta t_{matrix} \qquad \ldots(1)$$

or

$$\Delta t_{log} = (\Delta t_{liquid} - \Delta t_{matrix})\ \phi + \Delta t_{matrix} \qquad \ldots(1')$$

where Δt_{log} is transit time on the sonic log, Δt_{liquid} and Δt_{matrix} are transit times in formation liquid and matrix respectively, and ϕ is formation porosity. This equation means that, in rock of uniform lithology, transit time increases with porosity. Figure 2 shows the relationship between shale porosity, ϕ, derived from formation density logs, and shale transit time, Δt shale (μ sec/ft), from sonic logs, in the Cretaceous and Tertiary rocks of the area studied. Determination of shale porosity is based on the assumption that the grain density of the shale equals 2.65 gm/cc. The function obtained by the least-squares method is as follows:

$$\phi = 0.00472 \times \Delta t_{shale} - 0.362 \qquad \ldots(2)$$

By using equation (2), the transit time data from sonic logs can be converted to estimated porosity values.

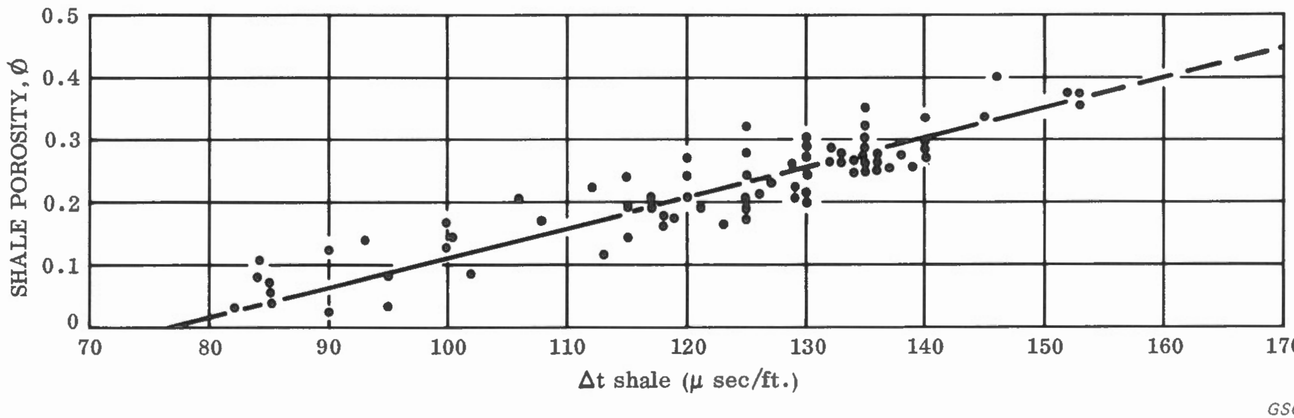

Figure 2. Relationship between porosity and transit time (Δt) of shale

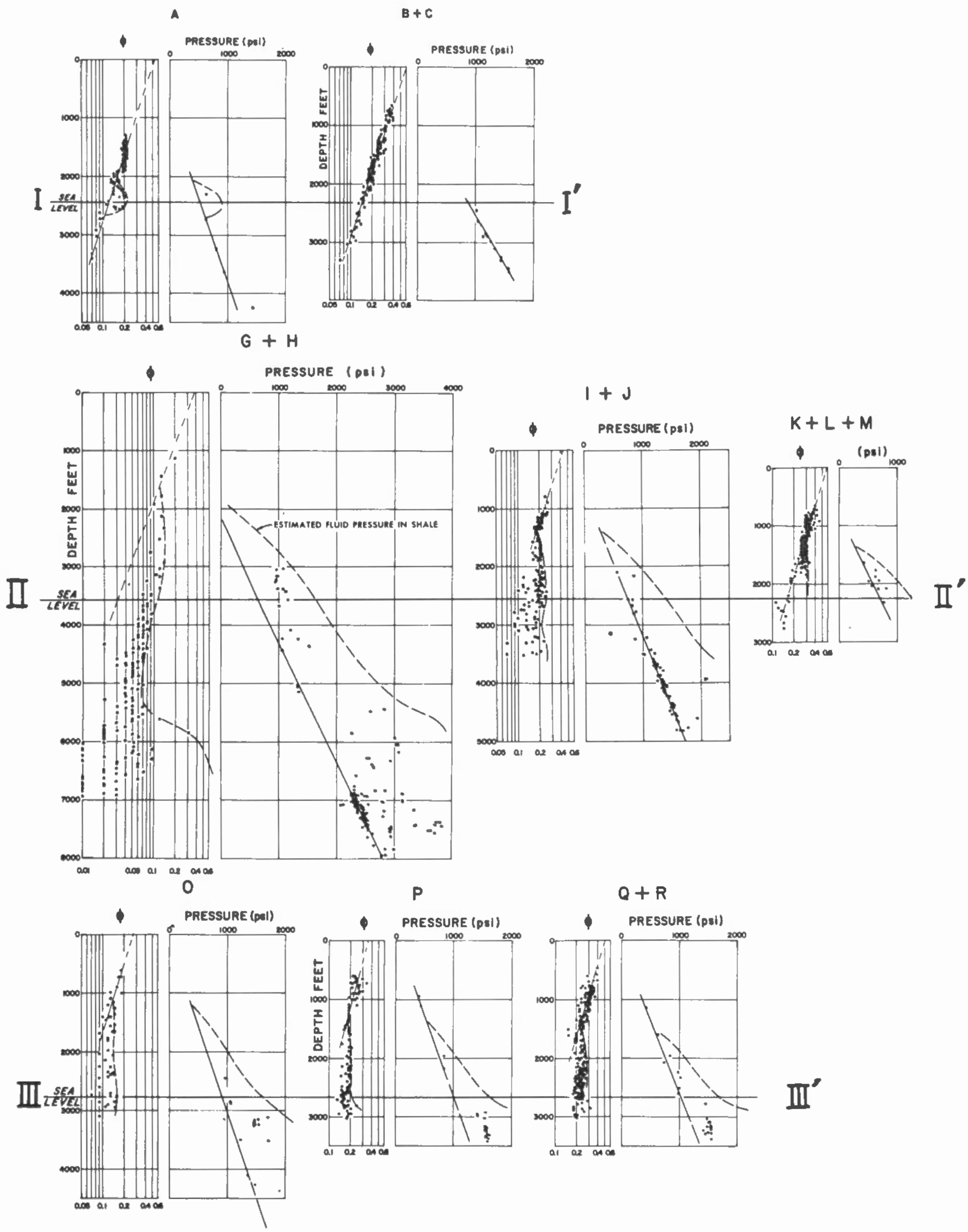

Figure 3. Comparison of shale porosity distribution and subsurface fluid pressure

For convenience, groups of wells close to each other have been considered as a single well and, in this paper, these groups are named A, B, ..., Y (Fig. 1). The vertical porosity distributions of Cretaceous and Tertiary shales in these groups have been determined by the use of sonic logs and are shown in figure 3 (the names of the wells used in this figure are listed in Table 2).

According to the shale porosity plots of figure 3, shale porosities decrease with depth and, on semi-log paper, porosity-depth relationships within relatively shallow depths are closely approximated by straight lines. At greater depths, however, the trend deviates toward higher porosity values. Figure 3 also shows the fluid pressure-depth relationships derived from the oil and gas wells in the same area. These pressure data are from both well completions and drillstem tests (Oil and Gas Conservation Board, 1967).

In the zones of abnormally high shale porosity (*see* Fig. 3), the fluid pressure is higher than the hydrostatic pressure, although the data are derived from different kinds of rock - sandstones and carbonates.

Hubbert and Rubey (1959) have demonstrated that the load, S, is supported jointly by the fluid pressure, p, and the grain-to-grain bearing stress, σ, of the clay aggregates:

$$S = \sigma + p. \qquad \ldots(3)$$

and load S can be expressed:

$$S = \bar{\rho}bw \cdot g \cdot Z \qquad \ldots(4)$$

where $\bar{\rho}bw$ is the mean value of the water-saturated bulk density of the overlying sediments, g is the acceleration of gravity, and Z is the depth of burial.

The grain-to-grain bearing stress, σ, exerted by the porous clay depends solely on the degree of compaction. The stress σ increases continuously as the porosity decreases (Rubey and Hubbert, 1959):

$$\sigma = f(\phi). \qquad \ldots(5)$$

If the shale porosity ϕ is abnormally high or the stress σ is abnormally low, the fluid pressure p should be abnormally high in order to support the overburden load S (equations 3, 4 and 5). The shale porosity distribution, therefore, is useful for predicting abnormal pressure (*see* Fig. 3).

The determination of abnormal pressure may be explained by means of the typical distribution of the vertical porosity of the shale, as shown in figure 4. A hydrostatic pressure environment prevails at shallow depths and an abnormal pressure at greater depths. The "normal porosity trend" line is drawn through the general average of the values plotted for the zone of hydrostatic pressure. When the porosity is plotted on the logarithmic scale and the depth on the arithmetic scale, the "normal porosity trend" line is commonly straight because of an exponential function between depth and porosity for the hydrostatic pressure condition[1]. As explained previously, the shale porosity values in the abnormal pressure zone are greater than the values the "normal porosity trend" would indicate. If the porosity of shale at depth Z in the abnormal pressure zone is equal to that at depth Ze on the "normal porosity trend" line, the grain-to-grain bearing stress is the same for both shales (*see* Fig. 4).

The overburden load, Se, and the fluid (hydrostatic) pressure, pe, at depth Ze can be shown as follows:

$$Se = \bar{\rho}bw \cdot g \cdot Ze \qquad \ldots(6)$$

$$pe = \rho w \cdot g \cdot Ze \qquad \ldots(7)$$

where ρw is the density of the formation water.

The function between the load, the stress of the clay and the fluid pressure at Ze is shown as follows (*see* equation 3):

$$Se = \sigma e + pe$$

or

$$\sigma e = Se - pe. \qquad \ldots(8)$$

Then, when equations (6) and (7) are introduced into equation (8), we obtain:

$$\begin{aligned}\sigma e = Se - pe &= \bar{\rho}bw \cdot g \cdot Ze - \rho w \cdot g \cdot Ze \\ &= (\bar{\rho}bw - pw)g \cdot Ze \qquad \ldots(9)\end{aligned}$$

---

[1] Rubey and Hubbert (1959), equation (15)

$$f = f_O \cdot e^{-cz},$$

where f is the shale porosity at depth z, f_O the shale porosity when $z=0$, e the base Napierian Logarithms, and c an exponential factor of dimension $(\text{length})^{-1}$.

(*see* Rubey and Hubbert, 1959, equation 10). The overburden load S at depth Z is shown as equation (4)[1]. As explained previously, the bearing stress σ at depth Z equals σe at depth Ze in the hydrostatic pressure zone, or

$$\sigma = \sigma e. \qquad \ldots(10)$$

From equations (3), (4), (9) and (10), the fluid (abnormal) pressure p at depth Z can be shown as:

$$\begin{aligned} p &= S - \sigma = S - \sigma e \\ &= \bar{\rho}bw \cdot g \cdot Z - (\bar{\rho}bw - \rho w) \cdot g \cdot Ze \\ &= \rho w \cdot g \cdot Ze + \bar{\rho}bw \cdot g \cdot (Z - Ze) \end{aligned} \qquad \ldots(11)$$

or

$$p^{(psi)} = 0.44 \times Ze^{(ft)} + 1.0 \times (Z - Ze)^{(ft)}. \qquad \ldots(11')$$

By using equations (11) or (11'), the shale porosity distribution can be converted to the fluid pressure distribution.

The curved broken lines in the fluid pressure sections of figure 3 show the possible maximum fluid pressures in shales as determined by the porosity distributions. The actual measured pressures in the reservoirs are sometimes lower than the maximum values derived from the shales. This can be explained by the greater permeability values (easier pressure depression) in the reservoirs.

POROSITY-PERMEABILITY RELATIONSHIP OF SHALE

Introduction

In discussing fluid movements in shales during compaction, a knowledge of shale permeability is essential. If the relationship between permeability and porosity can be determined, such discussion of fluid movements in a shale column will become easier, for several porosity-depth relationships for shales have already been proposed (Athy, 1930; Hedberg, 1936; Dickinson, 1951; Weller, 1959). There is, however, very little literature on the permeability-porosity relationship of shales (*see* Bredehoeft and Hanshaw, 1968). This is probably because: (1) most oil companies do not want to take any permeability data in

---

[1] The writer assumes that the mean water-saturated bulk density of the overlying sediments for depth Z approximates that for depth Ze.

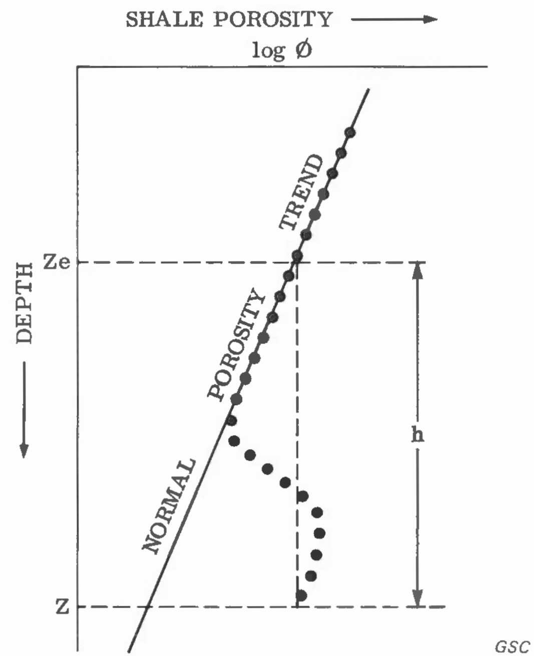

Figure 4. Schematic diagram showing porosity distribution in incompletely compacted shale

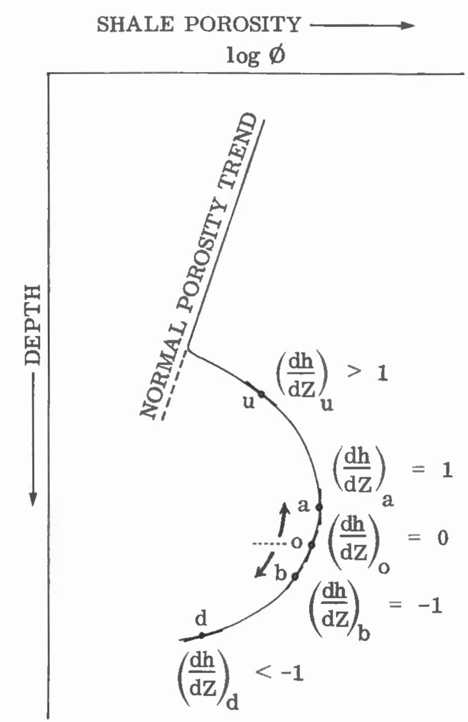

Figure 5. Schematic diagram showing slope changes of the porosity distribution in incompletely compacted shale

shales because of their low economic importance; (2) it is difficult to measure reasonable permeability values for shales because, although their original permeability tends to be low, this would be increased in well cores (shale) that may have some cracks or fissures caused by drilling; (3) it is not possible to estimate shale permeability in the subsurface by producing an appreciable amount of fluid from wells because shales normally produce no fluid.

Methods of estimating formation fluid pressure by well logs (Hottmann and Johnson, 1965; MacGregor, 1965; Wallace, 1965; Foster *et al.*, 1966; Fons and Holt, 1966; Rogers, 1966), which have been developed in the last few years, are based on an intimate relationship between pore fluid pressure and shale compaction or shale porosity. The study to be discussed here shows that the fluid pressure gradient in incompletely compacted shale can be determined also by the porosity distribution. It is possible, therefore, to determine permeability changes in shales by using the fluid pressure gradients and Darcy's law.

Having done this, the writer intends to estimate the permeability changes of Cretaceous shales in Alberta and Saskatchewan subsurface in this manner, then to combine shale porosity with permeability in order to investigate the relationship between them.

Fluid pressure gradients and movements of fluids in shales

As discussed previously, the value of abnormal fluid pressure at depth Z in the incompletely compacted shales as shown in figure 4 is given as follows:

$$p = \rho w \cdot g \cdot Ze + \bar{\rho} bw \cdot g \cdot (Z - Ze). \qquad \ldots(11)$$

This equation means that the abnormal pressure p at depth Z is equivalent to (the hydrostatic pressure at Ze) + (the overburden pressure between Ze and Z).

The abnormal fluid pressure p also can be expressed as follows (Hubbert and Rubey, 1959, equation 133):

$$p = pn + pa, \qquad \ldots(12)$$

where pn is the normal or hydrostatic pressure and pa a superposed anomalous pressure; pn is expressed as:

$$pn = \rho w \cdot g \cdot Z. \qquad \ldots(13)$$

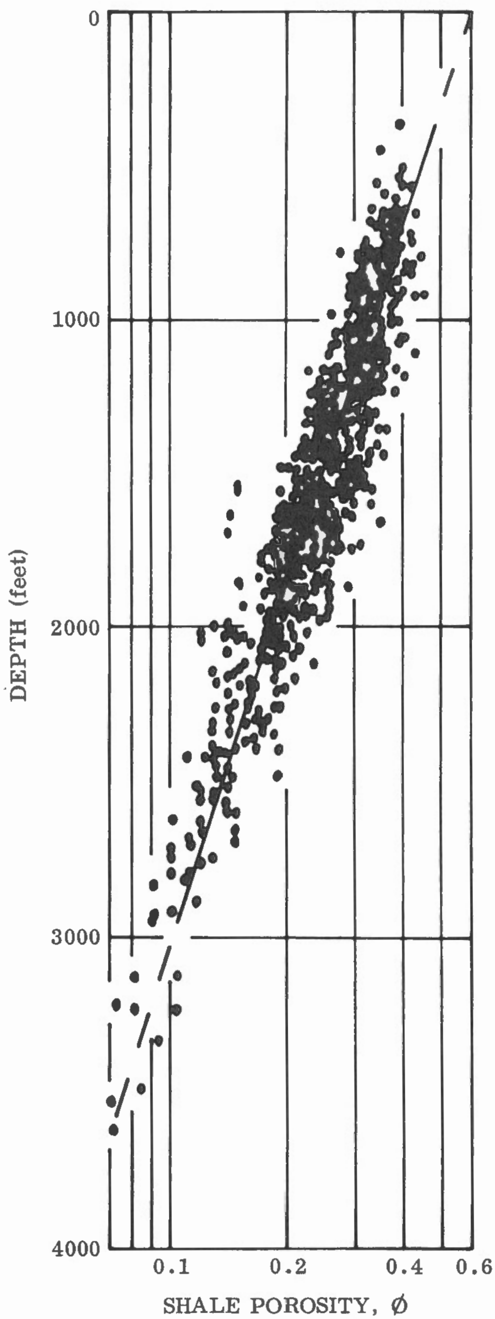

Figure 6. Normal shale porosity distribution in western Canada

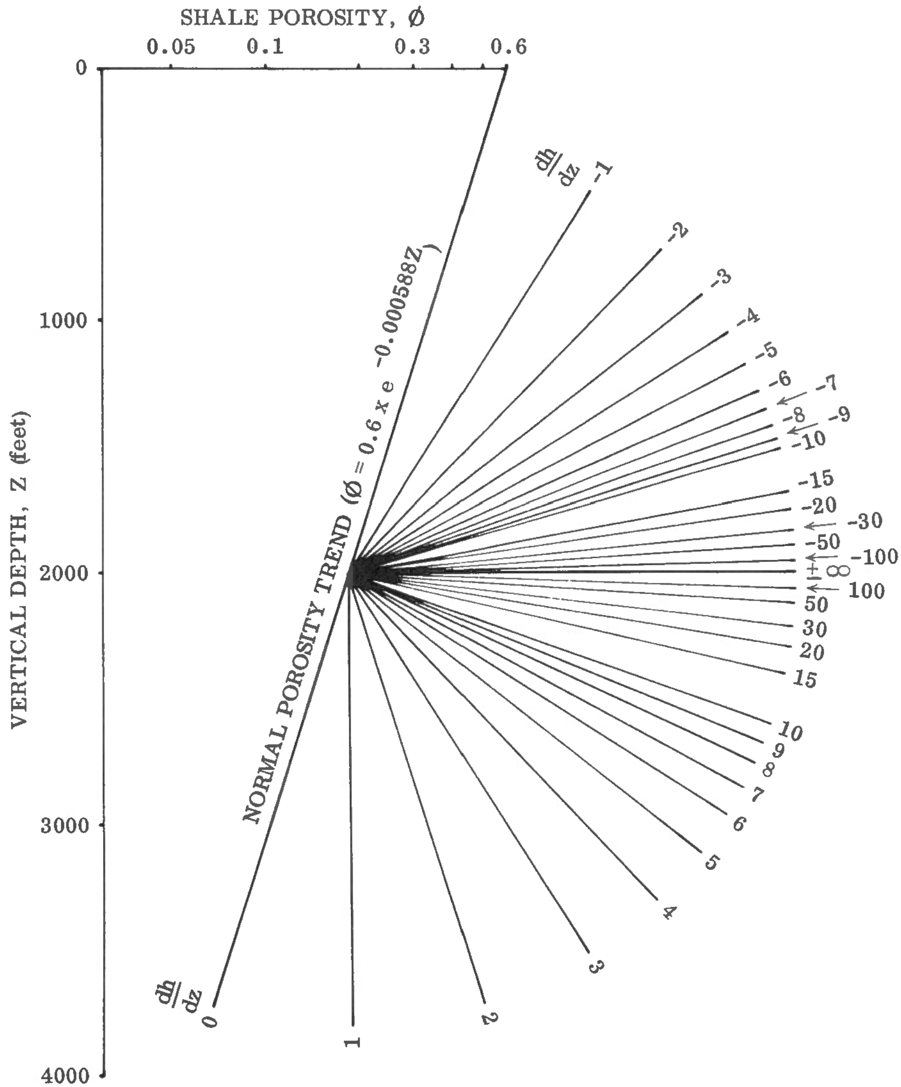

Figure 7. Chart for determining slope values of shale porosity distribution

From equations (11), (12) and (13), the anomalous pressure (excess pressure above the hydrostatic pressure) p_a can be shown to be:

$$pa = p - pn = \rho w \cdot g \cdot Ze + \bar{\rho}bw \cdot g \cdot (Z - Ze) - \rho w \cdot g \cdot Z$$
$$= (\bar{\rho}bw - \rho w) \cdot (Z - Ze) \cdot g. \qquad \ldots(14)$$

When, for convenience of description, we use a term h for (Z-Ze) (Fig. 4), we can express this simply as:

$$pa = (\bar{\rho}bw - \rho w) \cdot g \cdot h. \qquad \ldots(15)$$

Then

$$\frac{dpa}{dZ} = [(\bar{\rho}bw - \rho w)g] \frac{dh}{dZ}. \qquad \ldots(16)$$

$\frac{dpa}{dZ}$ is the anomalous pressure gradient and is equal to the change in anomalous pressure (above hydrostatic pressure) corresponding to a change in Z. $\frac{dh}{dZ}$ is the change in h corresponding to a change in Z.

Now, let us discuss the values of $\frac{dh}{dZ}$ in the typical incompletely compacted shales. As illustrated in figure 5, $\frac{dh}{dZ}$ is zero at point O, where the tangential line on the porosity curve in the incompletely compacted shales is parallel to the "normal porosity trend" line. This is expressed as follows:

$$\left(\frac{dh}{dZ}\right)_o = 0.$$

At point a, at which the tangential line is vertical, $\frac{dh}{dZ}$ equals 1. This is similarly shown as:

$$\left(\frac{dh}{dZ}\right)_a = 1.$$

Above point a, $\frac{dh}{dZ}$ increases upward and its value is greater than 1, or

$$\left(\frac{dh}{dZ}\right)_u > 1.$$

Below point O, $\frac{dh}{dZ}$ has negative values and decreases downward. Somewhere below point O, there must exist a point where $\frac{dh}{dZ}$ equals -1.(point b in Fig. 5), or

$$\left(\frac{dh}{dZ}\right)_b = -1.$$

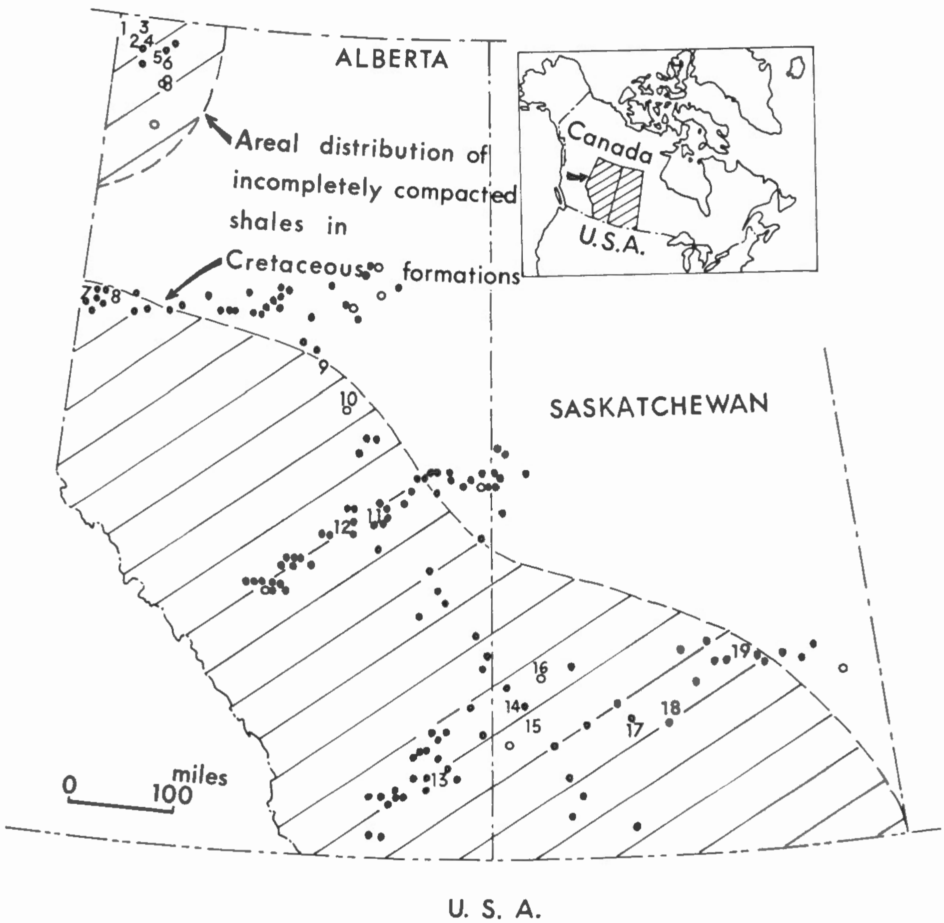

Figure 8. Index map showing well locations used in figures 9 and 10

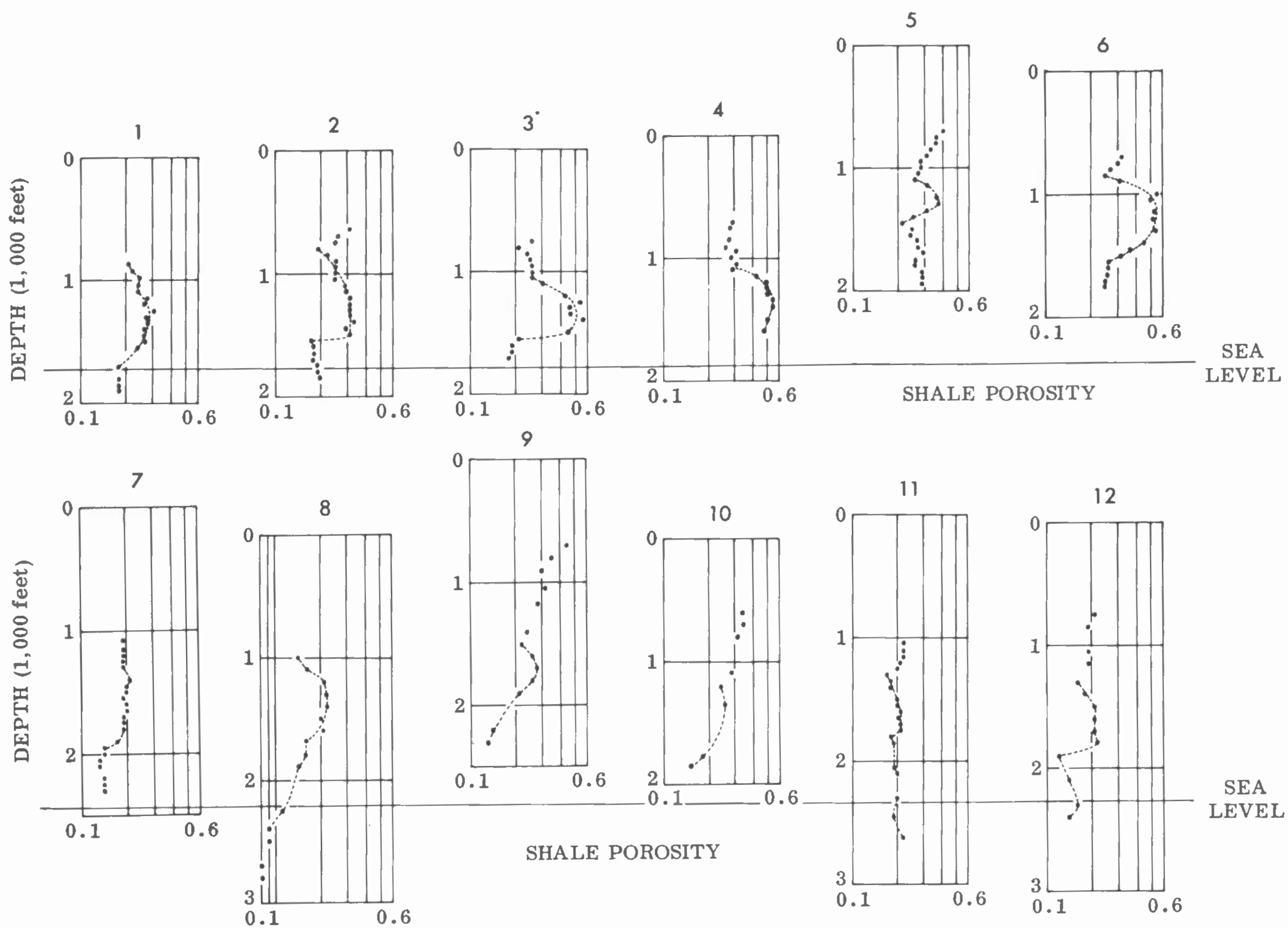

Figure 9. Examples of porosity distribution in incompletely compacted shale

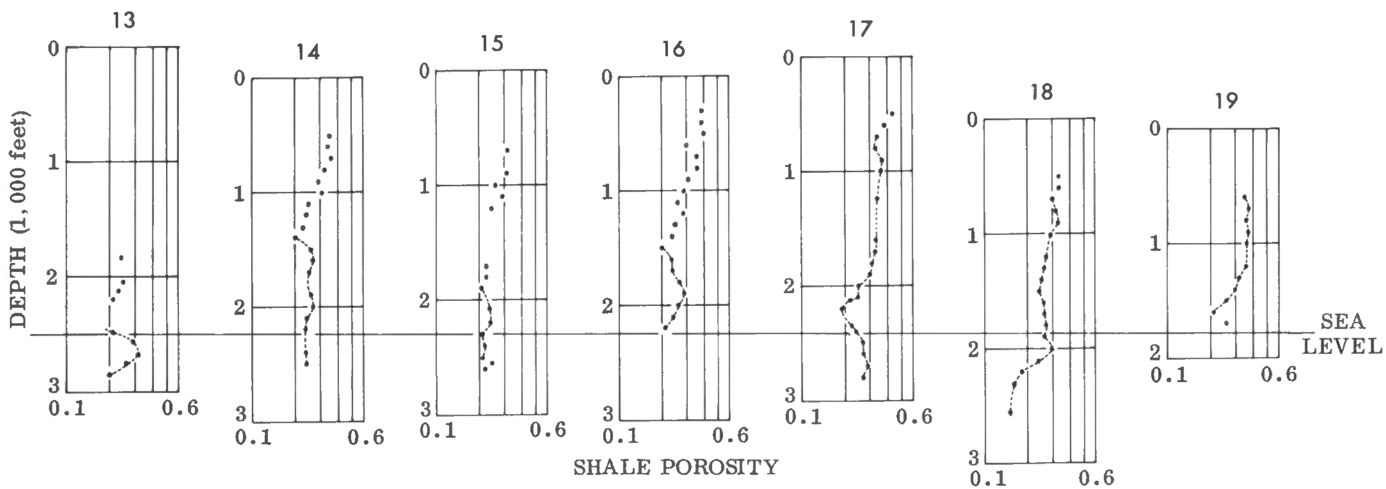

Figure 10. Examples of porosity distribution in incompletely compacted shale

Below point b, $\frac{dh}{dZ}$ values are given as follows:

$$\left(\frac{dh}{dZ}\right)_d < -1.$$

In the equations above, O, a and b denote the points O, a and b, respectively, and u and d denote the points in the upward and downward fluid-movement zones in the incompletely compacted shales.

As explained previously, $\frac{dh}{dZ}$ has a positive value above point O and a negative below. As the value of $(\rho bw - \rho w)g$ in equation (16) is always positive, $\frac{dpa}{dZ}$ has a positive value above point O and a negative value below. Fluid would move upward above point O and downward below. The volume of upward fluid movement qu crossing unit area normal to the flow direction in unit time is given by Darcy's law:

$$qu = -\frac{ku}{\mu u}\left(\frac{dpa}{dZ}\right)_u = -\frac{ku}{\mu u}(\bar{\rho}bw - \rho w)\cdot g\cdot\left(\frac{dh}{dZ}\right)_u, \qquad \ldots(17)$$

where ku and μu are, respectively, the permeability of shale and the viscosity of water at point u in the upward zone. As stated above, $\frac{dh}{dZ}$ at point a equals 1 (*see* Fig. 5). Hence, the volume of fluid movement qa at point a is given as follows:

$$qa = -\frac{ka}{\mu a}\left(\frac{dpa}{dZ}\right)_a = -\frac{ka}{\mu a}(\bar{\rho}bw - \rho w)\cdot g\cdot\left(\frac{dh}{dZ}\right)_a$$

$$= -\frac{ka}{\mu a}(\bar{\rho}bw - \rho w)g. \qquad \ldots(18)$$

In this case, qu and qa have negative values, and the following relationship would exist:

$$qu \leqq qa. \qquad \ldots(19)$$

From equations (17), (18) and (19) we obtain:

$$\frac{ka}{ku} \leqq \frac{\mu a}{\mu u}\left(\frac{dh}{dZ}\right)_u. \qquad \ldots(20)$$

As clearly seen in figure 5, the porosity value at point a is a maximum in the incompletely compacted shale zone, and the porosity decreases upward and downward. Supposing that there is a function between porosity and permeability of shale, and that the permeability decreases with decrease in porosity, the permeability value at point a would be greatest in this zone.

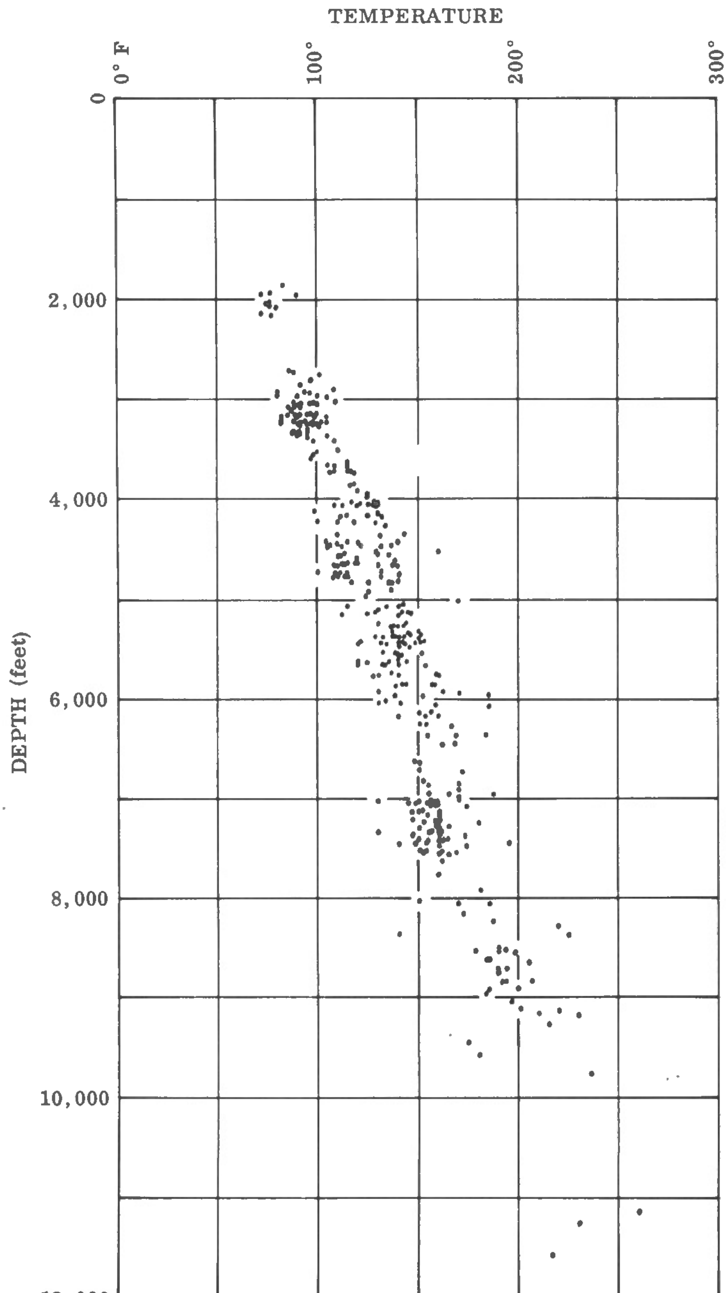

Figure 11. Temperature - depth relationship in Alberta

According to equation (20), the permeability ratio ka/ku can be calculated if the viscosity μa and μu of the formation fluid and $\left(\frac{dh}{dZ}\right)_u$ are known. It is possible to read the porosity values at the points a and u. Hence, the integration of the permeability values based on equation (20) with the porosity values is considered to be used to establish a relationship between shale porosity and permeability in the subsurface.

The volume of fluid movement qd in the downward zone is expressed as:

$$qd = -\frac{kd}{\mu d}\left(\frac{dpa}{dZ}\right)_d = -\frac{kd}{\mu d}(\bar{\rho}bw - \rho w)\cdot g\cdot\left(\frac{dh}{dZ}\right)_d, \qquad \ldots(21)$$

where d denotes a point below point b in the downward fluid movement zone. As the value of $\frac{dh}{dZ}$ at point b equals -1, the amount qb is shown as:

$$qb = -\frac{kb}{\mu b}\left(\frac{dpa}{dZ}\right)_b = \frac{kb}{\mu b}(\bar{\rho}bw - \rho w)g. \qquad \ldots(22)$$

In this case qd and qb have positive values and the following relationship would exist:

$$qd \geqq qb. \qquad \ldots(23)$$

From equations (21), (22) and (23) we obtain:

$$\frac{kb}{kd} \leqq -\frac{\mu b}{\mu d}\left(\frac{dh}{dZ}\right)_d, \qquad \ldots(24)$$

where $\left(\frac{dh}{dZ}\right)_d$ is always negative. The right-hand side of equation (24) is, therefore, positive ($\mu b/\mu d > 0$).

Equation (24) as well as equation (20) can be used to obtain the permeability ratio of shale in the subsurface. The integration of the permeability values based on equation (24) with the porosity values is used also to establish a relationship between shale porosity and permeability in the subsurface. The actual calculations in the Cretaceous shales in western Canada will be discussed below.

Porosity-permeability relationship of shale in western Canada

By using the method described above, a relationship between the porosity and permeability of Cretaceous shales in Alberta and Saskatchewan subsurface can be established.

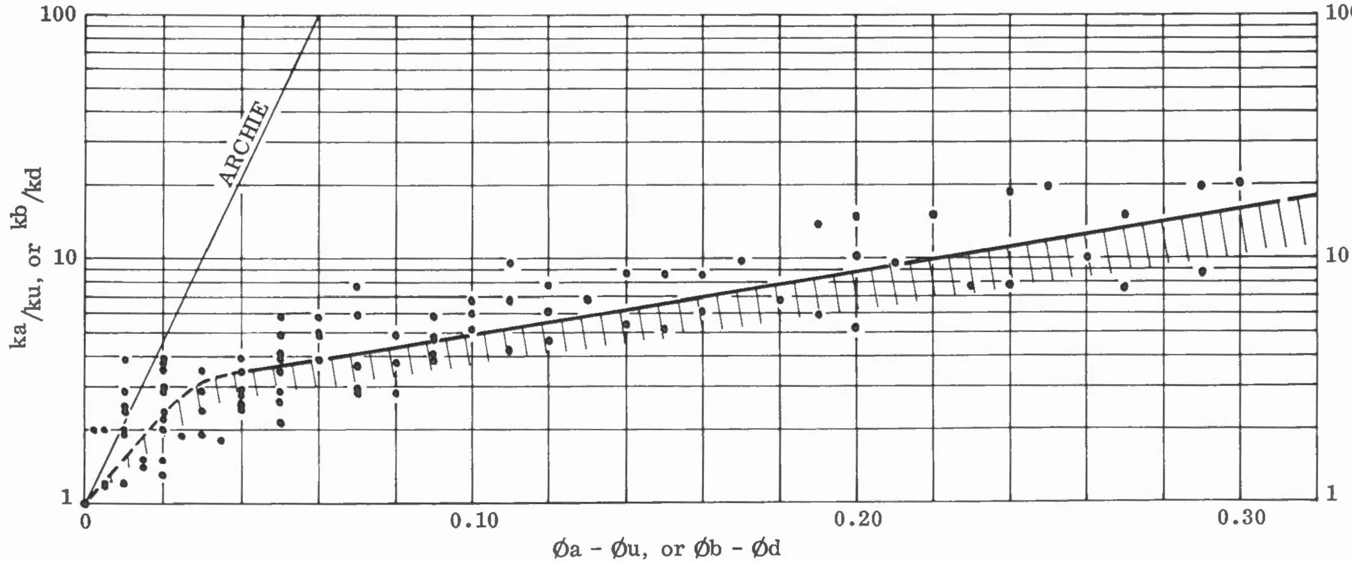

Figure 12. Relationships between permeability ratio and porosity difference of shale

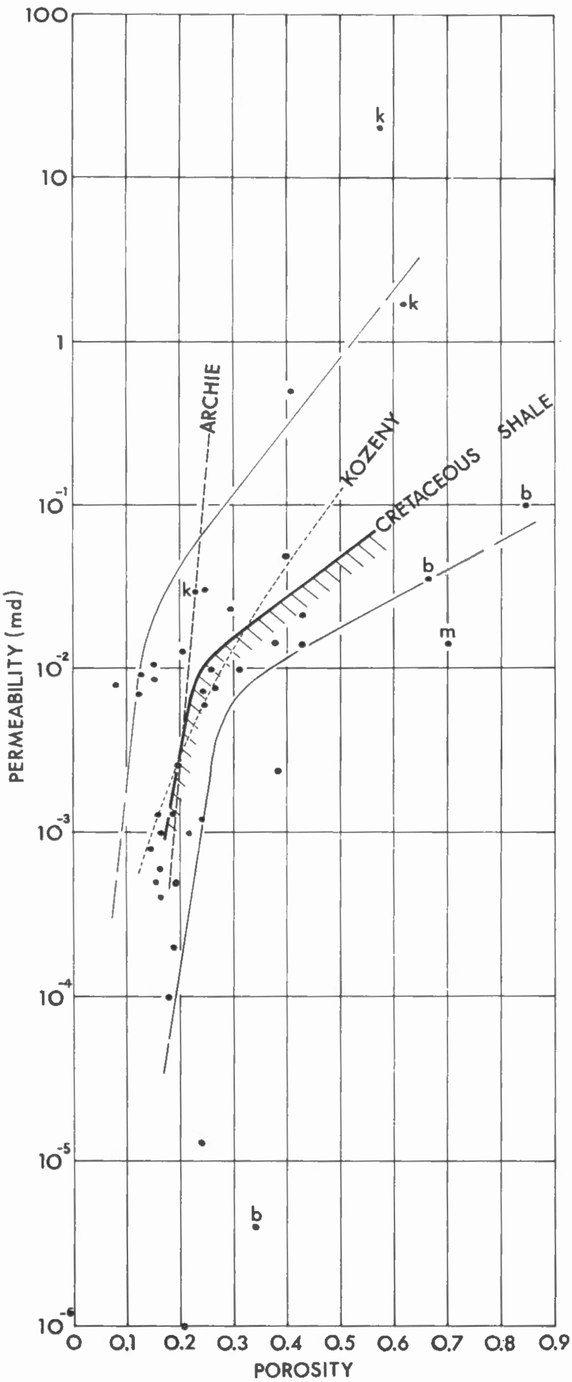

Laboratory-measured porosity-permeability data of shales, siltstones and clays in Canada, U.S.A., and Japan .... •
Kaolinite .... k
Montmorillonite .... m
Bentonite .... b

Figure 13.
Relationships between permeability and porosity of shale

As seen in figure 3, the "normal porosity trend" of shales in this area tends to shift to smaller values from east to west (shale porosity on the "normal porosity trend" at the same depth decreases from east to west, although the slope of the "trend" is almost constant). This decrease is attributed to the existence of a greater thickness of sedimentary rocks in the western part in the geological past which produced more compaction and to removal of a greater thickness of the uppermost part of the sedimentary column in the west. After the erosion thickness has been compensated for, the "normal porosity trend" in this area is determined (*see* Fig. 6). The function of the "normal porosity trend" of Cretaceous and Tertiary shales in the area studied is expressed as follows:

$$\begin{aligned}\phi &= 0.6 \times e^{-0.000588z(ft)} \\ &= 0.6 \times e^{-0.0000193z(cm)}\end{aligned} \qquad \ldots(25)$$

The values of $\frac{dh}{dZ}$ based on the "normal porosity trend" in western Canada are illustrated in figure 7. By using this figure, $\frac{dh}{dz}$ values in the incompletely compacted shale zones are easily determined.

The next step is to read the $\frac{dh}{dZ}$ values of the incompletely compacted shales in the Alberta and Saskatchewan subsurface. For this purpose, 35 wells have been chosen in the area where the Cretaceous formations have incompletely compacted shales (*see* Figs. 9 and 10 for shale porosity).

The viscosity of the formation water would change mainly with temperature. The writer assumes that the average geothermal gradient in this area is 1.8° F per 100 feet of depth, and that the subsurface temperature at 2,000 feet is 75° F, based on the temperature-depth data in Alberta (Oil and Gas Conservation Board, 1967, Fig. 11). The viscosity of the formation water at each depth based on this temperature data is determined by assuming that the dissolved solids content of water equals 40,000 mg/l (*see* Pirson, 1963, Figs. 4-6). The ratios ka/ku and kb/kd are calculated by equations (20) and (24) respectively, and the porosities ϕa, ϕu, ϕb, and ϕd at these points are read.

Figure 12 shows the plots of ka/ku or kb/kd (logarithmic scale) against $\phi a - \phi u$ or $\phi b - \phi d$ (arithmetic scale), when the equal signs in equations (20) and (24) are established. The average relationship in this case is shown as a curved solid line. The actual ka/ku or kb/kd values, however, according to equations (20) and (24), would be smaller than these plotted values. The relationship between ka/ku or kb/kd and $\phi a - \phi u$ or $\phi b - \phi d$ would, therefore, be expressed by the shadowed area in figure 12.

Archie (1950) proposed a porosity-permeability relationship for sandstones, limestones and muddy sands. According to this relationship, an increase in porosity of about 3 per cent produces a tenfold increase in permeability. Archie's relationship is shown as a straight line in figure 12, where the increase in shale permeability with increase in porosity is less than that given by Archie's relationship, which is based on sandstone and carbonate rocks.

Comparison of log-derived and laboratory-derived porosity-permeability relationships

Data on permeability-porosity relationships of shale are at present very scarce but much of what is available has been compiled by Bredehoeft and Hanshaw (1968). The Geological Survey of Japan has measured the permeabilities and porosities of the mudstone cores of several stratigraphic test wells in Japan, and the writer has obtained similar data on a well in the Strathmore gas field in Alberta. The data for Japan and Alberta are listed in table 3 and shown in figure 13.

In figure 13, Archie's porosity-permeability relationship, mentioned above, is shown as a straight broken line (Archie), and Kozeny's (based on sandstones) is shown as a curved broken line (Kozeny, *see* Pirson, 1963). The log-derived porosity-permeability relationship in western Canada, when the equal signs in equations (20) and (24) are established, is illustrated as a curved solid line (Cretaceous shale). The actual relationship is shown by the shaded area in figure 13. The starting point for these three lines (Archie, Kozeny, and Cretaceous shale) in this figure is located at the point of porosity 0.2 (or 20%) and permeability 3×10^{-3} md. Although the data are derived from several different areas, figure 13 shows that the log-derived porosity-permeability relationship is more applicable for shales than are the Archie and Kozeny relationships.

CAUSES OF ABNORMAL PRESSURES

Introduction

Reservoir pressures in the subsurface usually approximate hydrostatic pressure, which equals the weight of the water column from reservoir to surface. A pressure that materially exceeds the weight of an equivalent column of water is "abnormal", and a pressure materially less is "subnormal" (Levorsen, 1954). Reservoir pressure can not exceed the weight of the overlying rock column, or geostatic pressure.

Dickinson (1953) reported an instance of abnormal pressure in the Gulf Coast equal to 0.87 times the geostatic pressure, and Kok and Thomeer (1955) cited an example of 0.90 times. More data on abnormal pressures have been compiled by Rubey and Hubbert (1959). Dickinson (1953) also reported the first recognized association of abnormal pressures with the relative proportions of sand and shale in a geologic column. Abnormal pressures can be influenced also by the mean formation permeability, the elapsed time since deposition, the rate of deposition, and the amount of overburden (Hottmann and Johnson, 1965).

According to Thomeer and Bottema (1961), favorable conditions for abnormal pressures in thick shale sequences may be found in younger sedimentary basins where the rapid deposition of shales over considerable areas did not allow time for hydrostatic equilibrium to be reached. With respect to the common occurrence of abnormal pressures in more deeply buried shale successions, Rubey and Hubbert (1959) advanced the following explanation: "When the rate of sedimentation is somewhat greater, pore water may still escape rapidly enough to maintain an essentially hydrostatic pressure in the relatively porous mudstone at shallow and intermediate depths but not in the more compacted and therefore less permeable rock at greater depths". In a significant recent contribution, Powers (1967) suggested a new interpretation of the origin of abnormal fluid pressure in the deep subsurface based on the application of current knowledge of clay-colloid chemistry and mineralogy. According to Powers, the alteration of montmorillonite to illite begins at a depth of about 6,000 feet and continues at an increasing rate to a depth usually about 9,000 - 10,000 feet, where no montmorillonite is left. The alteration offers a mechanism for desorbing the last few layers of bound water in clay and transferring it as free water to interparticle locations. These last few layers of bound water have a considerably greater density than free water, and water increases in volume as it is desorbed from between unit layers. As the water expands, it increases the pore fluid pressure to abnormally high levels.

Several possible explanations of abnormal fluid pressure in the relatively deeper parts of sedimentary sequences are discussed below.

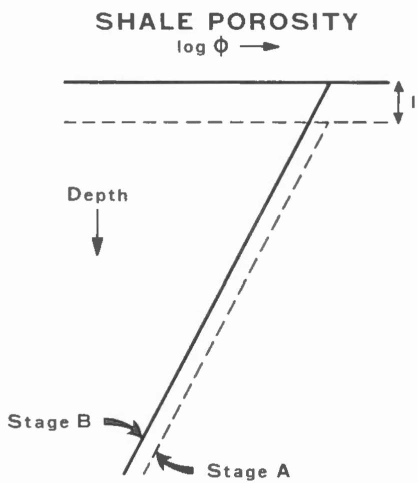

Figure 14. Schematic vertical porosity distributions of shale at equilibrium condition of compaction

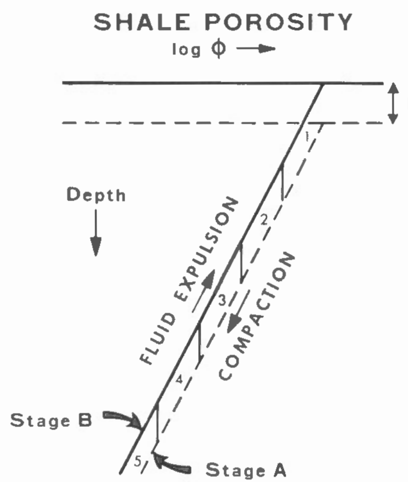

Figure 15. Diagram showing compaction of shales and fluid expulsion in case of additional sedimentation

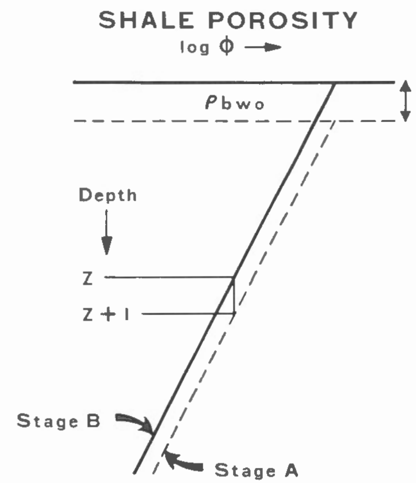

Figure 16. Schematic vertical porosity distributions of shales at equilibrium condition of compaction

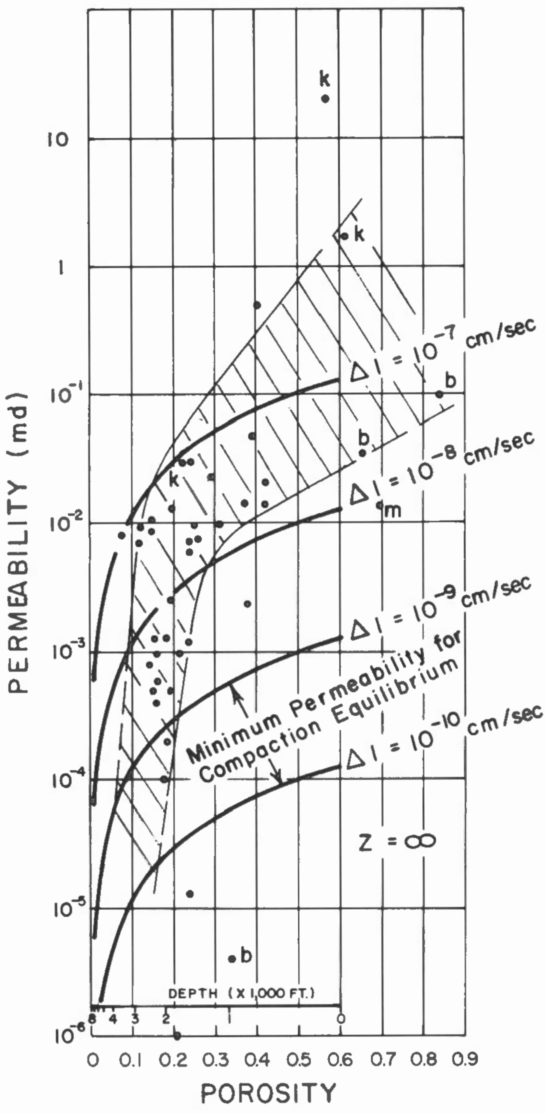

Laboratory-measured porosity-permeability data of shales, siltstones and clays in Canada, U.S.A., and Japan .... •

Kaolinite .... k

Bentonite .... b

Montmorillonite .... m

Thickness of sediments is infinite in this case (or Z = ∞)

Figure 17. Diagram showing minimum shale permeability for compaction equilibrium and actual permeability of shale

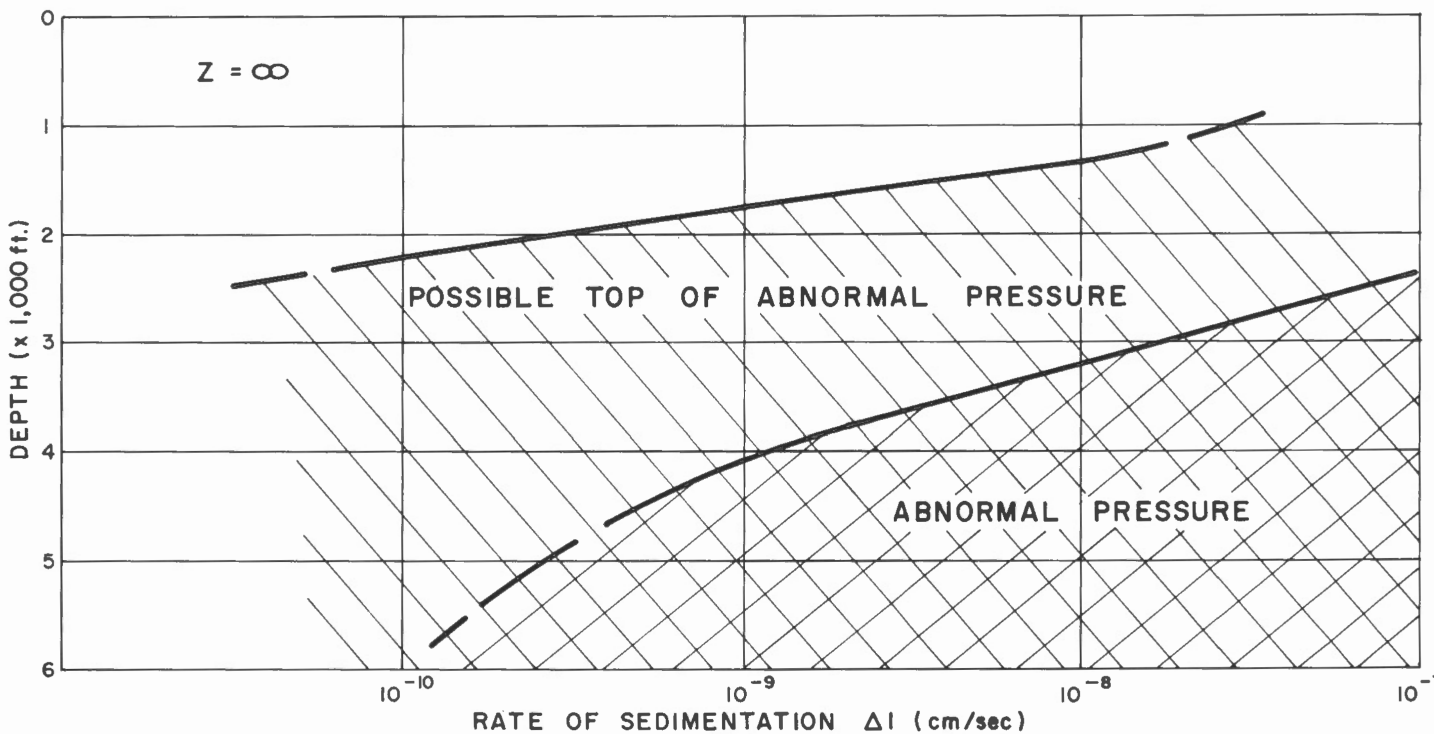

Thickness of sediments is infinite in this case (or $Z = \infty$)

Figure 18. Showing calculated top of abnormal pressure zone at different sedimentation rates

Expulsion of fluids from shale during subsidence

The existence is assumed of a clay or shale sequence in which the clay or shale has reached a compaction equilibrium and within which the fluid pressure is hydrostatic (Stage A of Fig. 14). Additional marine sediments are added at the top and the sequence subsides an amount, l, in a time interval, t. If the entire shale reaches a new equilibrium condition of compaction after the subsidence of l, a porosity distribution such as shown by stage B in figure 14 would be established. As explained previously, an exponential function exists between shale porosity and depth at the equilibrium condition in western Canada.

Suppose that an outlet for fluid expulsion exists only at the surface, and the fluid is expelled upward. In this case the compaction of the shale from stage A to stage B would occur from the shallower to the deeper part of the sequence (Fig. 15). This figure shows schematically that the porosity decrease occurs from the shallower part to the deeper (from 1 to 5). In considering fluid migration under this circumstance, the fluid pressure gradient between stages A and B must be determined, and figure 16 has been constructed for this purpose. In this situation, the fluid pressure difference P_l between depth Z on the stage B line (hydrostatic pressure) and depth $Z + l$ on the stage A line (abnormal pressure) is given as:

$$P_l = S_l = \rho bwo \cdot g \cdot l, \qquad \ldots(26)$$

where S_l is the overburden pressure increase in this case and ρbwo is the water-saturated bulk density of shale at the surface (below water level). When the fluid pressure increase is resolved into two components (Hubbert and Rubey, 1959, equations 133 and 134),

$$P_l = Pln + Pla$$

or

$$P_{la} = Pl - Pln, \qquad \ldots(27)$$

where P_{ln} is the normal or hydrostatic pressure increase and P_{la} a superposed anomalous pressure increase. In this case P_{ln} is shown as:

$$Pln = \rho w \cdot g \cdot l. \qquad \ldots(28)$$

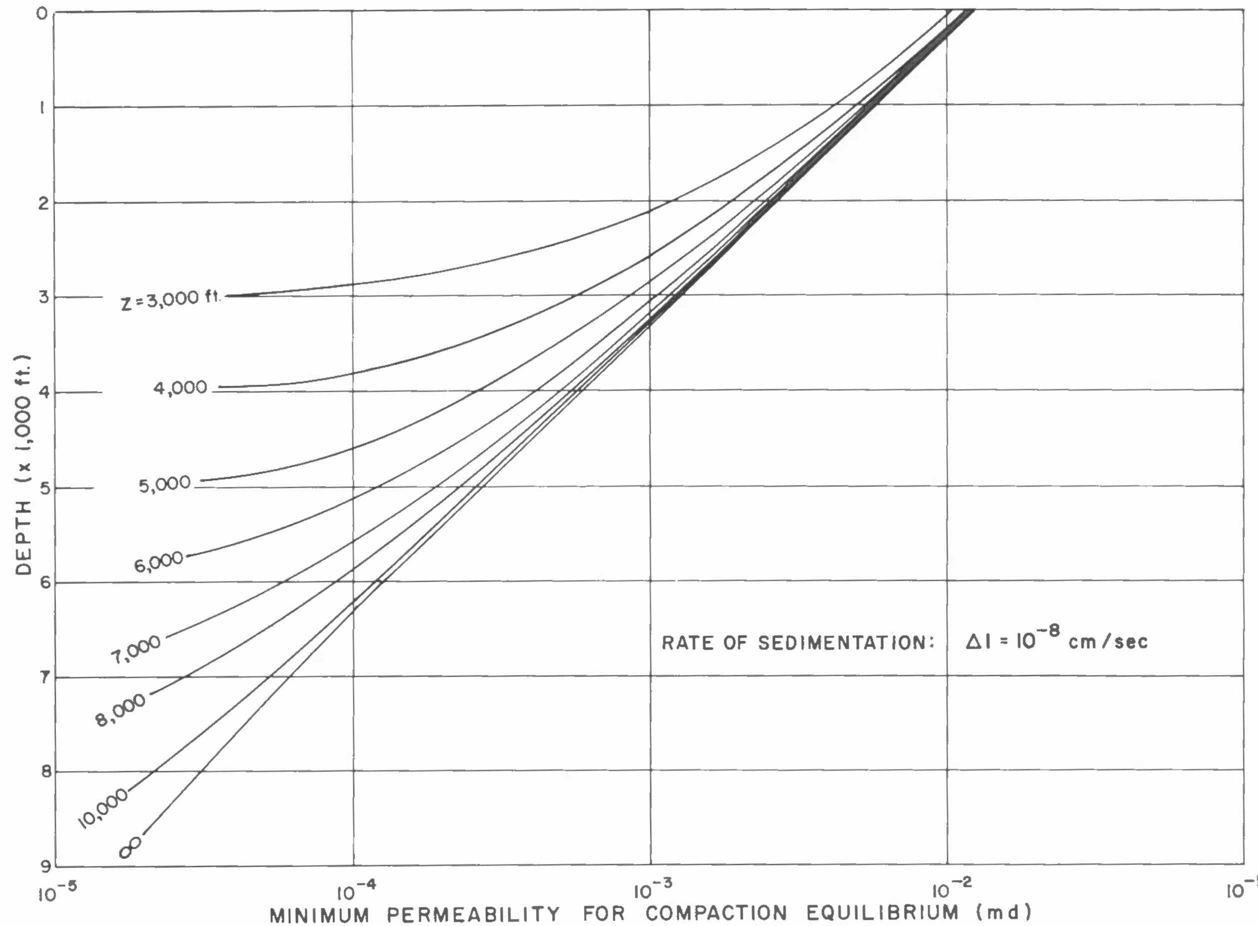

Figure 19. Relationship between minimum permeability for compaction equilibrium and total thickness of sediment

From equations (26), (27) and (28), P_{la} can be expressed as follows:

$$Pla = (\rho bwo - \rho w)g \cdot l \qquad \ldots(29)$$

or

$$\frac{Pla}{l} = (\rho bwo - \rho w)g. \qquad \ldots(30)$$

The anomalous pressure gradient in the situation shown in figure 16 is given by equation (30).

Fluid movement in this case is shown by Darcy's law (*see* also equation 17):

$$q = \frac{k}{\mu} \cdot \frac{Pla}{l}, \qquad \ldots(31)$$

where q is a volume of water crossing unit area normal to the flow direction in unit time, k the permeability of shale, and μ the fluid viscosity. The volume of water q_1 passing depth Z_1 in unit time in a shale column is expressed from equations (30) and (31) as:

$$q_1 = \frac{k_1}{\mu_1} \cdot \frac{Pla}{l} = -\frac{k_1}{\mu_1}(\rho bwo - \rho w)g, \qquad \ldots(32)$$

where the subscript 1 denotes depth Z_1, and q_1 is considered to be the volume of water passing through the shale at depth Z_1, whose permeability is k_1. The volume of the passing water Q_1 in time interval t is given as:

$$Q_1 = q_1 \cdot t = \frac{k_1}{\mu_1}(\rho bwo - \rho w)g \cdot t. \qquad \ldots(33)$$

Assuming that the shale compaction occurs simply by the expulsion of fluids from the shales, the porosity difference in figure 16 indicates the amount that should be expelled between stages A and B for the new equilibrium of compaction to be reached. Supposing that the direction of fluid expulsion in this case is upward, the amount that should pass through the shale at depth Z_1 can be calculated.

An exponential function between shale porosity and depth at the equilibrium condition of compaction proposed by Rubey and Hubbert (1959, equation 15) is as follows:

$$\phi = \phi_o \cdot e^{-cz}, \qquad \ldots(34)$$

where ϕ is the value of shale porosity at depth Z, ϕ_o the porosity when $Z=0$, e the base Napierian logarithms, and C a constant of dimension $(\text{length})^{-1}$. The line of the stage A in figure 16 could be shown mathematically by equation (34). Suppose that the subsidence l occurs in time interval t and the shales reach a new equilibrium condition of compaction (Stage B in Fig. 16). The porosity-depth relationship in this case is shown as:

$$\phi + \phi_l = \phi_o \cdot e^{-c(z + l)}, \qquad \ldots(35)$$

where ϕ_l is the porosity difference between stage A and B. From equations (34) and (35),

$$\phi_l = \phi_o \cdot e^{-cz} \cdot (e^{-cl} - 1). \qquad \ldots(36)$$

In this case the total amount of porosity decrease in a shale column with the unit base area is given by the integral of equation (36) as follows:

$$\int \phi_l dz = \phi_o (e^{-cl} - 1) \int e^{-cz} dz. \qquad \ldots(37)$$

This amount of the porosity decrease is here considered to be the volume of fluids that must be expelled from the shale column for the new equilibrium to be reached. As this volume normally tends to go upwards, the volume that should pass through depth $Z1$ for the equilibrium is expressed as:

$$\int_{z1}^{z} \phi_l dz = \phi_o (e^{-cl} - 1) \int_{z1}^{z} e^{-cz} dz. \qquad \ldots(38)$$

Z in equation (38) is considered to be the bottom depth or the thickness of the shale sequence.

When this volume is equal to or less than Q_1 in equation (33), sufficient fluid is expelled from the shales and a hydrostatic-pressure environment is established. When it is greater than Q_1, on the other hand, some fluid remains and an abnormal pressure occurs. In the case where this volume is balanced with Q_1 in equation (33), the following relationship exists:

$$Q_1 = -\frac{k_1}{\mu_1}(\rho bwo - \rho w) g \cdot t = \phi_o (e^{-cl} - 1) \int_{z1}^{z} e^{-cz} dz. \qquad \ldots(39)$$

In this equation k_1 is considered to be the minimum permeability for the new compaction equilibrium to be reached, and is given as:

$$k_1 = \frac{\mu_1 \cdot \phi_o}{(\rho bwo - \rho w) g \cdot t}(1 - e^{-cl}) \int_{z_1}^{z} e^{-cz} dz. \qquad \ldots(40)$$

If the average subsidence or sedimentation rate in time interval t is given as Δl, the following relationship would exist:

$$l = t \cdot \Delta l. \qquad \ldots(41)$$

When we take a certain time interval (for example, 1 second) for t in equations (40) and (41), we can calculate k_l at several sedimentation rates.

Using equations (40) and (41), the minimum permeability for compaction equilibrium can be determined for several rates of sedimentation Δl. Calculations have been made on the assumption that ρbwo and ρw in the area studied are 1.67 and 1.02 (gm/cc) respectively. ϕ_0 is assumed to be 0.60 (60%). The viscosity of the formation water is determined from the temperature data in the plains (*see* Fig. 11). The minimum permeabilities for compaction equilibrium when the sedimentation rate Δl is 10^{-7}, 10^{-8}, 10^{-9} and 10^{-10} cm/sec are illustrated in figure 17. The permeability is plotted on the logarithmic scale (ordinate) and the porosity on the arithmetic scale (abscissa). In this case the bottom depth or total thickness of the shale sequence is infinite. The depth scale corresponding to the scale porosity value on the "normal porosity trend" (Fig. 6) is also shown on the abscissa. In figure 17, the laboratory-measured porosity and permeability data of shales and clays from table 3 or figure 13 are plotted also. As explained previously, these porosity and permeability data were obtained from several different formations in different areas, which means that this porosity-permeability relationship does not represent one particular area, but could be used to arrive at a general porosity-permeability relationship for shale. Such a relationship can, therefore, be shown by the shaded area in figure 17.

In this figure, the minimum permeability line when $\Delta l = 10^{-8}$ cm/sec intersects the actual permeability zone between 0.27 (or 27%) and 0.09 (or 9%) porosity. The porosity values correspond to depths of about 1,300 feet and 3,200 feet, respectively, on the "normal porosity trend" of western Canada. In depths shallower than 1,300 feet (or porosity greater than 0.27), the actual permeability would be greater than the minimum for compaction equilibrium to be reached, when the sedimentation rate Δl equals 10^{-8} cm/sec. In this case, enough fluid for the equilibrium can be expelled from the shale and a hydrostatic pressure condition would be established. At greater depths, the actual permeability would be less than the minimum for equilibrium. Some fluids would remain in this part of the sequence and an abnormal pressure would occur.

Figure 18 is a plot of the possible top of the abnormal pressures at several sedimentation rates; it shows that when the rate of sedimentation is high the abnormal pressures would occur at relatively shallow depths.

The previous discussions are based on the assumption that the bottom of the shale sequence exists at an infinite depth, or $Z = \infty$, in equation (40). What would happen if the bottom lay at a relatively shallow depth with an impermeable base? Figure 19 shows the minimum permeability vs. depth when the bottom depth Z = 3,000 feet, 4,000 feet ---------10,000 feet and ∞ ($\Delta l = 10^{-8}$ cm/sec). According to this figure, the minimum permeability for equilibrium at the same depth increases as the bottom depth Z increases. This means that the thicker the entire shale sequence, the greater the possibility of abnormal pressures developing.

In the Cretaceous formations of western Canada, the abnormal pressures occur mainly in the western parts of the plains (Fig. 3), where the thickness is greater and sedimentation was more rapid. This high rate of sedimentation and great total thickness are considered to be possible causes of the abnormal pressures in this part of the plains.

Clay mineral alteration

In order to examine the possibility of montmorillonite dehydration proposed by Powers (1967), data was obtained on the clay-mineral contents of several well cores. Because the detailed studies on the topic are continuing, only one example in western Canada will be given here.

Figure 20 shows the data on core porosity, sonic porosity and mineral content of shales. Figure 20A illustrates the shale core porosity-depth relationship of the Strathmore 7-12-25-25W4 well in Alberta (Fig. 1). The porosity is calculated from the dry density of the cores, assuming that the grain density of the shales equals 2.65 gm/cc. Because this well does not have any sonic-log data, the closest well in which a sonic log was run (Arden 6-4-25W4) has been chosen for comparison (Fig. 20B). Figure 20B shows the porosity-depth relationship of this well based on the shale porosity - Δt relationship in the plains (Fig 2). Both core and sonic porosities fit fairly well. According to figures 20A and B, abnormally high shale porosities exist below about 800 feet.

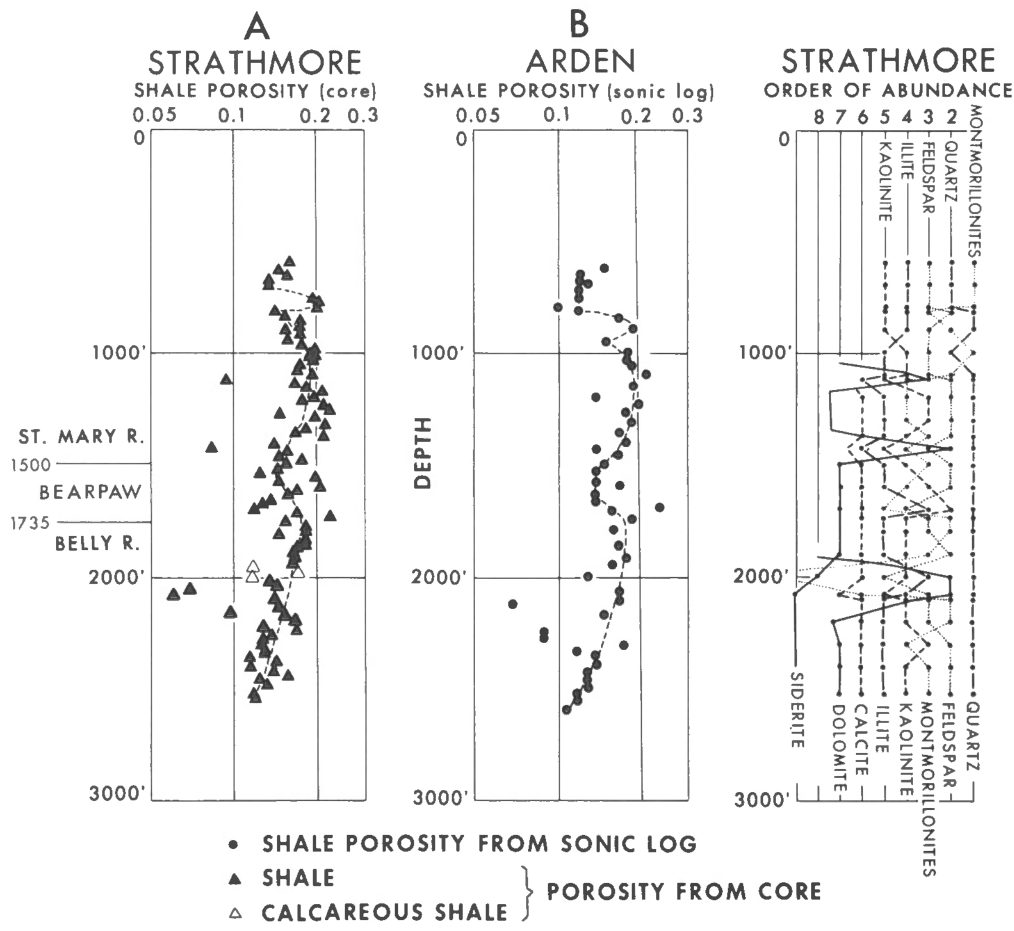

Figure 20. Comparison of shale porosity and mineralogy

The results of clay mineral studies of the Strathmore cores, made by A.E. Foscolos at the Geological Survey of Canada, Calgary, are given in order of abundance of several clays (Table 4). The right-hand picture of figure 20 shows this result most clearly. At a depth of about 1,000 feet, the abundance of montmorillonite seems to drop and kaolinite seems to increase. Illite, however, does not increase at this depth.

As a result of the shale compaction study now in progress in western Canada the estimated thickness of the eroded formations in the geological past is about 1,400 feet at this location. The maximum depth to the top of the montmorillonite increase would have been at a depth of about 2,400 feet at this location. This estimated depth is considered to be much shallower than the depth of montmorillonite dehydration proposed by Powers (1967).

AMOUNT OF FLUIDS EXPELLED FROM CRETACEOUS SHALES IN NORTHEASTERN BRITISH COLUMBIA AND NORTHWESTERN ALBERTA

Introduction

Shale compaction occurs mainly because of the expulsion of fluids from the shales and also can be influenced by adjacent permeable rocks such as sandstones and carbonates. This problem has been discussed using well-log data in Nagaoka Plain, Japan (Magara, 1968a). In the Japanese Tertiary rocks, sharp porosity decreases occur in the shales close to the permeable reservoir rocks. This is explained as follows. The fluids in the shales are easily expelled into the adjacent permeable rocks resulting in the compaction of the shales and a decrease in porosity. However, if the rocks adjacent to the shales are not permeable or lenticular, the fluids are not expelled and no porosity decrease is observed. Therefore, the decrease of shale porosity may be used as an indicator for the permeabilities of the adjacent reservoir rocks.

The difference in porosity between the initial and the present stage indicates the volume of fluids expelled from the shales to the reservoir rocks in the geological past. Since some of these fluids possibly contained petroleum, the discussion of this subject is quite useful and important for petroleum exploration.

The amount of fluids expelled downward from the Cretaceous shales to the underlying sandstones and carbonates in British Columbia and the northwestern part of Alberta is discussed below. This particular area has been chosen because of the incompletely compacted shales in the Cretaceous formations and the various hydrocarbon pools in the Cretaceous and adjacent formations.

Porosity distributions of Cretaceous shales

About 300 wells, all with sonic logs, have been studied in British Columbia and northwestern Alberta (*see* Fig. 21), and their names and locations are listed in table 5. Shale porosity of the Cretaceous formations has been determined from the sonic logs using the relationship of porosity and transit time shown in figure 2. The vertical shale porosity distributions along lines A-A', B-B', C-C', D-D', E-E', F-F', and G-G' (Fig. 21) are shown in figures 22, 23, 24, 25, 26, 27 and 28, respectively.

As explained above, the abnormally high porosity (or incompletely compacted) shale is commonly associated with abnormally high fluid pressure. In a vertical shale column, the fluid moves from a point of higher anomalous pressure (higher excess pressure over the hydrostatic) to a point of lower anomalous pressure. The directions of fluid migration in a schematic shale porosity distribution have been discussed previously (*see* Fig. 5).

The curved broken lines in figures 22-28 indicate the boundary surfaces between upward and downward fluid migration in the shales. This boundary surface is determined by the concept developed in an earlier section of this report; below it, the fluid moves downward to the underlying rocks. The thickness of the downward migration zone normally increases westward. Abrupt porosity decreases in the shales close to the reservoir rocks occur mainly in the western part of the area, suggesting that the underlying rocks have relatively higher permeabilities and the fluid would have migrated to them relatively easily from the shales. In the eastern parts, such porosity decreases are not clear, suggesting that the underlying rocks have relatively lower permeabilities.

The object of this study is to calculate the volume of fluid expelled downward from the shales to the underlying reservoir rocks. As a first step, however, an isopach map of the downward migration zone in the shales (Fig. 29) has been constructed; this map also shows locations of oil and gas pools in the underlying rocks (Lower Cretaceous, Jurassic and Triassic formations). As seen in figure 29, most of these oil and gas pools are in the area where the downward migration zone is thicker than 500 feet.

A method of calculating the volume of fluid expelled in the geological past has been developed by Magara (1968a) and is used here. Assuming that the shale grain before and after burial is the same, the following relationship obtains:

$$V \cdot (1 - \bar{\phi}) = V' (1 - \bar{\phi}'), \qquad \ldots (42)$$

where V and V' are the respective shale volumes, and $\bar{\phi}$ and $\bar{\phi}'$ the respective average porosity values, before and after burial. First, the present (after burial) vertical porosity distribution of shale, as shown schematically in figure 30, is established. In calculating the volume of the downward migration, the present (after burial) volume V' of the downward migration zone per unit vertical column of the shales, and the present average porosity $\bar{\phi}'$ of the zone, are necessary.

However, the porosity distribution at any time in the geological past (before burial) is unknown. It is assumed that this porosity distribution conformed to the "normal porosity trend" of the shales, implying that at that time fluid could be expelled from the shales rather easily and a hydrostatic pressure prevailed. By assuming a "normal porosity trend" for the porosity distribution before burial, the average porosity $\bar{\phi}$ in this zone is known. The shale volume V (before burial) is given as,

$$V = V' \frac{(1 - \bar{\phi}')}{(1 - \bar{\phi})}. \qquad \ldots (43)$$

A volume of fluid expelled downward, Wd, can be calculated as,

$$Wd = \overline{\Delta\phi} \cdot V = (\bar{\phi} - \bar{\phi}') \; V' \frac{(1 - \bar{\phi}')}{(1 - \bar{\phi})}. \qquad \ldots (44)$$

This method is applied to the area studied.

Figure 31 shows the volume of fluid expelled downward from the Cretaceous shales to the underlying rocks, as well as the locations of oil and gas pools in the underlying reservoirs. Most oil and gas pools are concentrated in the area where the greater volume of fluid is considered to have been expelled.

The previous discussions have taken into account only the volume of the downward migration from the overlying shales to the reservoirs. Upward migration from the underlying source rocks also might have played some role in the formation of hydrocarbon pools in the reservoirs. It is believed, however, that hydrocarbons produced from the overlying shales could have been entrapped in the reservoirs more effectively because the overlying shales are important also as cap rock. It is doubtful that the cap rock overlying the reservoirs was present at the time the fluids from underlying shales were expelled upward. The overlying source shales thus seem to be more important in hydrocarbon accumulation and the present study therefore was confined to them.

COMPACTION EXPERIMENT USING CLAYS

Introduction

Several compaction experiments have been conducted on clays and the results reported (Chilingar and Knight, 1960; Meade, 1966; Engelhardt and Gaida, 1963). Most of these works, however, were concerned with the compaction of clays and the changes of water salinity during compaction, and hence used relatively small specimens. Therefore, they are not suitable for determining the porosity distributions inside the clay.

The object of the present experiments is to obtain porosity patterns in several clays at several stages of compaction. An apparatus for this purpose was constructed by the Geological Survey of Canada in Calgary.

Apparatus for compaction experiments

Figure 32 shows the apparatus that was devised for the compaction experiments. It is composed of a metal base (a) and a brass tube 2 inches in diameter (b) divided into ten 2-inch segments. Brass plates (c) are welded to the top and bottom of each segment: the brass bolts (d), which hold the segments together, permit the removal of individual segments, and rubber rings between the segments prevent water leakage. Metal plates (e) also are placed between the segments and they are used for slicing the clays. Above the ten segments is a cylinder (f) containing a brass piston (g) with a rubber tip. The piston may be systematically loaded at (h) to a maximum weight of 400 pounds. In experimental compaction, the cylinder and the ten segments are filled with water-saturated clays of various compositions. During progressive loading, water is expelled through the top (i) and bottom (j) outlets. Two sandstone cores are placed at the top and bottom of the clays.

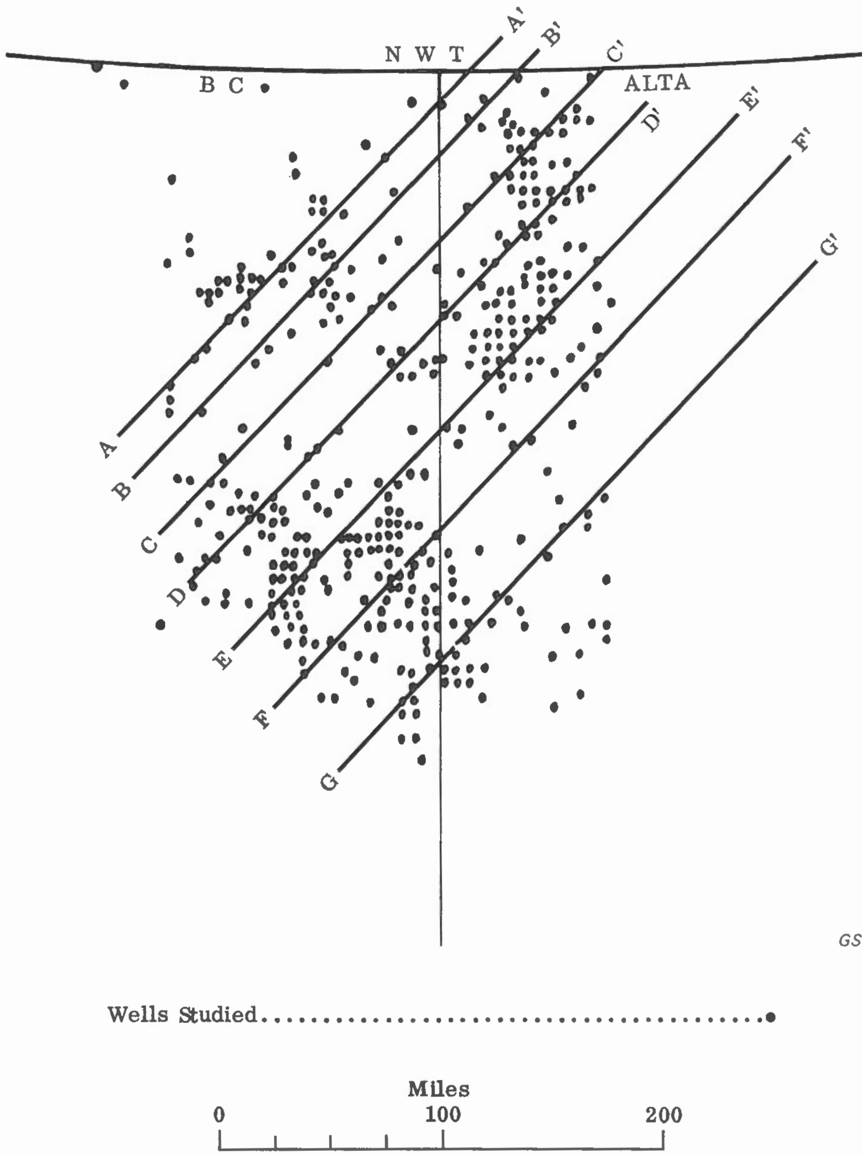

Figure 21. Index map of wells used for detailed compaction study (Table 5) and shale porosity profile lines

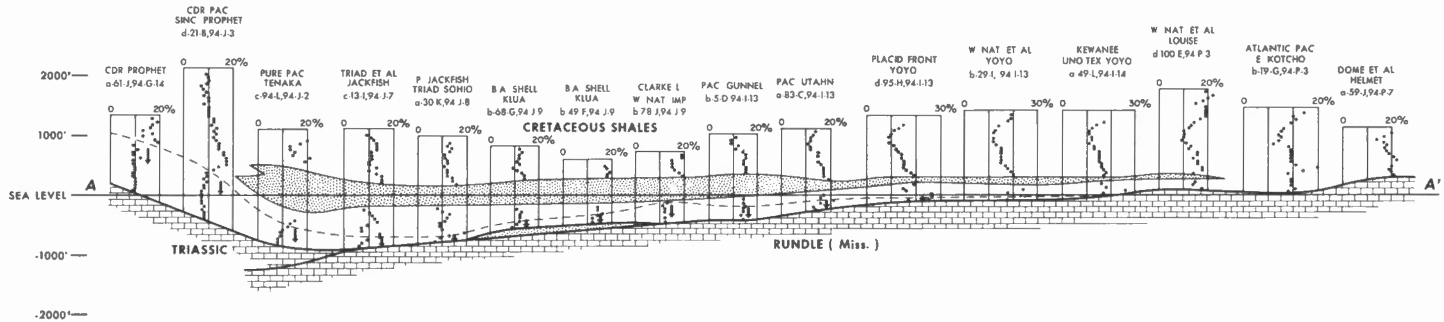

Figure 22. Profile showing shale porosity distribution along A - A'

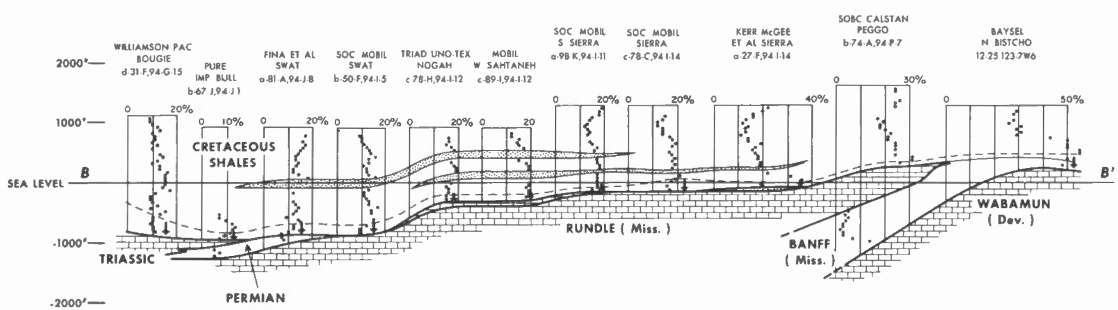

Figure 23. Profile showing shale porosity distribution along B - B'

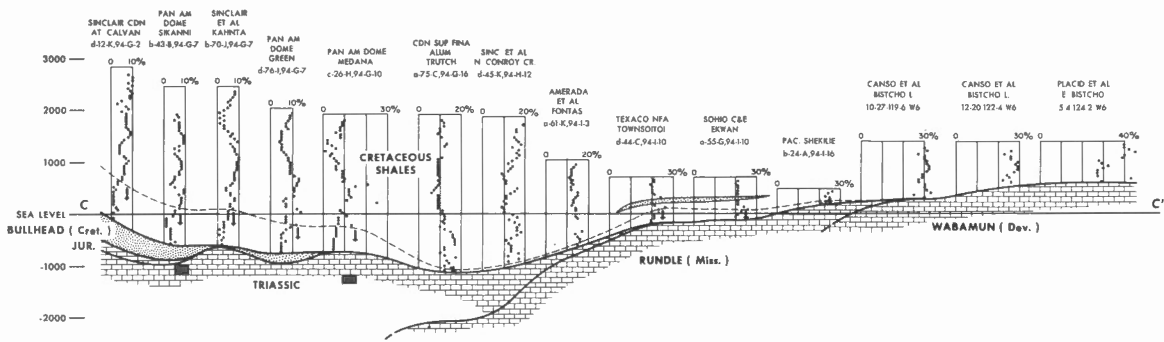

Figure 24. Profile showing shale porosity distribution along C - C'

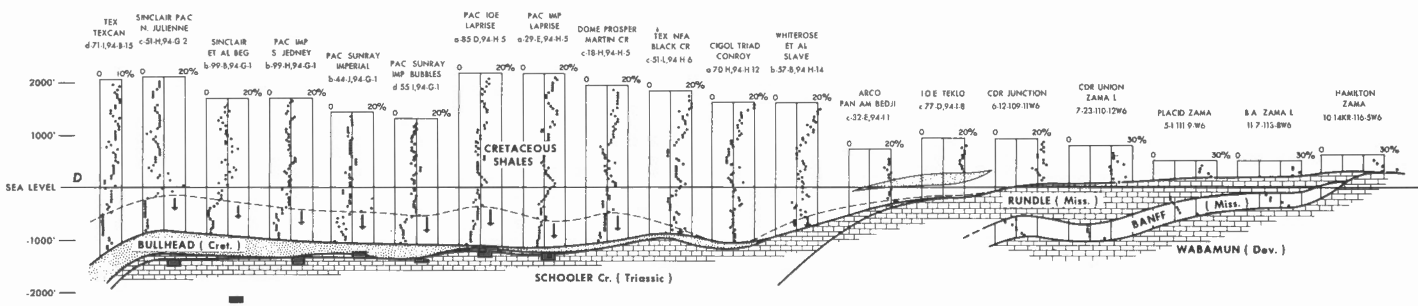

Figure 25. Profile showing shale porosity distribution along D - D'

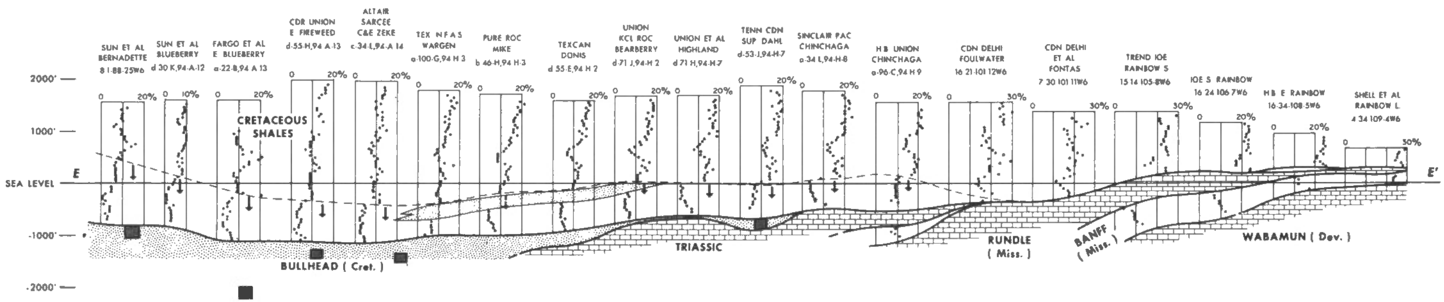

Figure 26. Profile showing shale porosity distribution along E - E'

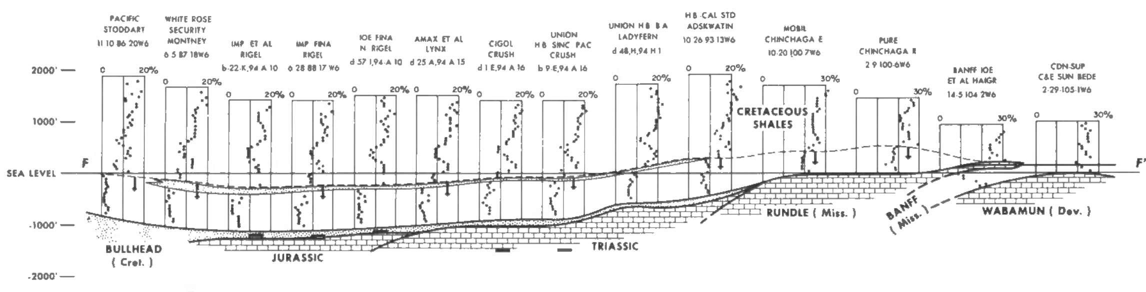

Figure 27. Profile showing shale porosity distribution along F - F'

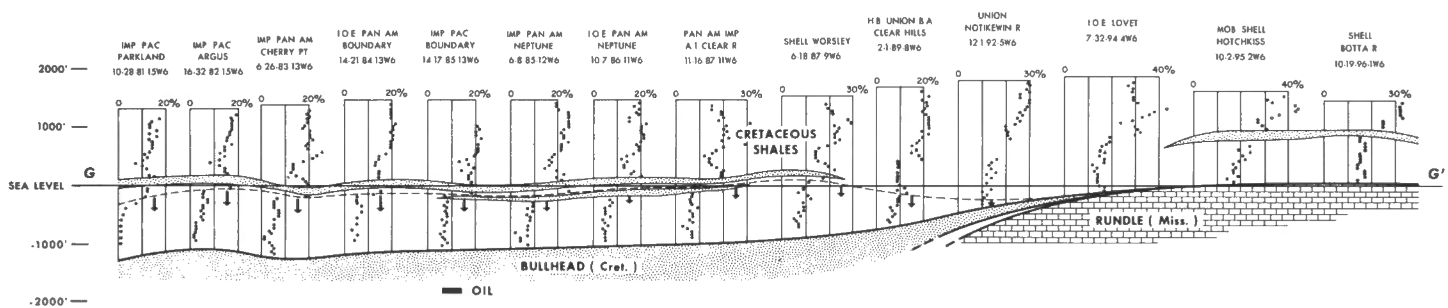

Figure 28. Profile showing shale porosity distribution along G - G'

Method of experiment

The inner volume and the empty weight of each segment (b) are first measured. After a segment has been filled with water-saturated clay, it is weighed again; the difference in weight is the weight of the water-saturated clay. The bulk density ρbw of the clay can then be determined by dividing this weight by the internal volume of the segment. Porosity is calculated by using the following equation:

$$\rho bw = \phi \cdot \rho w + (1 - \phi) \cdot \rho g$$

or

$$\phi = \frac{\rho g - \rho bw}{\rho g - \rho w}, \qquad \ldots(45)$$

ρg of the clays is assumed to be 2.65 gm/cc. The initial porosity of clays in each segment is calculated by equation (45). Following this the ten segments, a metal base, a cylinder and a piston are put together. The piston is loaded to a weight of 400 pounds.

When compaction has taken place and water is expelled from the clays, the ten segments are removed and the weight of each, including the clays, is measured. Porosity distribution at this stage is determined.

By repeating such measurements, porosity patterns at different stages of compaction can be determined. New clays are added at the top of the clays (in the cylinder), and compaction experiments proceed.

Results of experiments

A: Montmorillonite[1]:

Both top and bottom outlets are open, simulating the presence of permeable sandstones above and below a shale sequence. The clay was saturated with about 1.5N NaCl solution. Results are shown in figure 33. Large porosity decreases occur at both ends, close to the outlets; the decrease in the middle, on the other hand, is relatively slow.

---

[1] Montmorillonite No. 25,
John C. Lane Tract,
(Bentonite)
Upton, Wyoming

B: Montmorillonite[1]:

This time, the bottom outlet is closed, simulating impermeability of the underlying sandstone (Fig. 34). A large porosity decrease occurred at the uppermost part of the clay, close to the top outlet. Between stages 2 and 3, the height of the piston was measured periodically; the results are shown in figure 35. There seems to be an exponential function between piston height and time, indicating that the compaction slows down with time.

C: Montmorillonite[1]:

The bottom six segments were initially filled with salt-water-saturated (2N NaCl) montmorillonite, while the cylinder and top four segments were filled with fresh-water-saturated montmorillonite. This simulates deposition in saline-water conditions followed by fresh-water conditions. More water was expelled from the bottom or salt-water side than from the top or fresh-water side. In other words, in this situation more water was squeezed out downward than upward. The results are shown in figure 36.

D: Kaolinite[2]:

In this case the top and bottom outlets were open. The bulk density or porosity difference is relatively small (*see* Fig. 37).

E: Montmorillonite-Kaolinite:

Seven segments from the bottom were initially filled with kaolinite and the cylinder and three segments from the top with montmorillonite. This time both top and bottom ends were open. In segments 4 and 5, the porosity increased from stage 1 to stages 2 and 3. This is because the montmorillonite, which has a higher porosity, was pushed down during this experiment (*see* Fig. 38).

F: Illite[3]:

The results for illite are shown in figure 39. The porosity difference under this weight (400 lb.) is very small.

G: Montmorillonite-Illite:

The results of this experiment are shown in figure 40. In this case, the major porosity difference occurred in montmorillonite. Porosity in the illite part is small at stage 1 and very little change occurred during the experiment.

---

[1] Ibid.

[2] Kaolinite No. 4
Macon, Georgia

[3] Illite No. 35
Fithian, Illinois, 48W1535

TREND OF FUTURE RESEARCH

Introduction

The calculation of the volume of fluids expelled downward from the Cretaceous shales to the underlying rocks could be practically useful for petroleum exploration, because if this volume is large, the amount of hydrocarbons also may be large. In this calculation, it is assumed that the initial porosity distribution conforms to the present "normal porosity trend". However, this is not necessarily true in every case, although the semi-quantitative volume of fluids expelled in the geological past might tell something about the possibility of finding oil and gas, and the properties of the reservoir rocks, such as permeability.

In order to discuss the volume of fluids expelled, the porosity patterns of incompletely compacted shales at several stages of compaction should be known. In other words, the compaction process in incompletely compacted shales should be clearly understood. Once this process is known, the volume of fluids expelled during a certain geological time can be calculated.

Volume of fluids expelled downward and upward

The log-derived porosity-permeability relationship is shown by the shaded area in figure 12. This means that the present study could not obtain a single function between shale porosity and permeability, but obtained some range between them. However, the relationship between $\frac{\mu a}{\mu u}\left(\frac{dh}{dZ}\right)_u$ or $-\frac{\mu b}{\mu d}\left(\frac{dh}{dZ}\right)_d$ in equation (20) and (24) and $(\phi a - \phi u)$ or $(\phi b - \phi d)$ can be expressed as a single curved line (Fig. 41). By using both figures 41 and 7, the slopes of the shale porosity curves at each $(\phi a - \phi u)$ or $(\phi b - \phi d)$ are determined and the ideal shale-porosity curves in the incompletely compacted shale zone can be constructed.

Figure 42 shows such examples of the constructed porosity distributions (A: ϕa = 0.6 or 60%; B: ϕa = 0.5 or 50%; C: ϕa = 0.4 or 40%; D: ϕa = 0.3 or 30%; E: ϕa = 0.2 or 20%). The values of $\frac{\mu a}{\mu u}$ and $\frac{\mu b}{\mu d}$ are assumed in this case to be 1 ($\mu a = \mu u$, or $\mu b = \mu d$). Superposition of the curves in figure 42 may suggest the porosity distribution at several stages of compaction, but the porosity differences in the upward and downward fluid movement zones, from one stage to another, must fit the volumes of fluid expelled upward and downward between these stages.

The ratio qu/qd is expressed as follows (*see* equations 17 and 21):

$$\frac{qu}{qd} = \frac{ku}{kd} \cdot \frac{\mu d}{\mu u} \cdot \frac{\left(\frac{dh}{dZ}\right)u}{\left(\frac{dh}{dZ}\right)d}, \qquad \ldots(46)$$

Supposing that $\left(\frac{dh}{dZ}\right)_u$ and $\left(\frac{dh}{dZ}\right)_d$ values are taken at the points of the same porosity value in both upward and downward zones (Fig. 43) and the permeability values of two shales are the same when porosity values are the same, equation (46) is reduced to:

$$\frac{qu}{qd} = \frac{\mu d}{\mu u} \cdot \frac{\left(\frac{dh}{dZ}\right)u}{\left(\frac{dh}{dZ}\right)d}, \qquad \ldots(47)$$

The ratio of the volumes of upward and downward fluid movement can be determined by equation (47).

The values of qu/qd when the maximum porosity ϕa equals 0.6, 0.5, ... 0.2 are determined from figure 42 and equation (47) and the average values are shown in figure 44 (qu/qd - ϕa relationship). Figure 44 shows a general tendency of qu/qd to decrease with a decrease in ϕa. This means that the relative volume of the downward fluid movement against the upward increases with compaction of the shales.

Figure 45 shows a superposition of the porosity curves, in which the porosity differences in the upward and downward fluid movement zones between two stages of compaction fit these qu/qd ratios. The area between two curves shows the volumes of fluids expelled from the unit shale column during these two stages of compaction. The area above line 0-0' represents the volume of upward fluid expulsion, while the area below represents the volume of downward expulsion. The volumes per unit vertical shale column, whose base area is 1 square foot, are shown also in figure 45.

The study of the volumes of fluids expelled in different stages, as discussed above, may be useful for exploration of hydrocarbons if this information is tied with the timing of the trap configuration.

Shale porosity distribution as an indicator for permeability of reservoir rocks

The slope of the porosity curve in the incompletely compacted shale zone indicates the anomalous fluid pressure gradient in the shales. The integration of this pressure gradient and Darcy's law reveals the permeability of the rocks.

Figure 46 is constructed to explain this situation. To the left is a schematic shalè porosity distribution, in which incompletely compacted shales exist at depth. Suppose that fluid is expelled upward from the sequence: in this situation, the volume of fluids, q, passing vertically through the sequence would gradually increase upward (*see* the right-hand side of Fig. 46). Because this increase is considered to be quite gradual, we may obtain an instant idea of the average permeability of the rocks by the porosity distribution of the shales. According to Darcy's law, the following relationship exists:

$$q = -\frac{k}{\mu} \cdot \frac{dpa}{dZ}. \qquad \text{...(50)}$$

In zones A, C and E of figure 46, $\frac{dh}{dZ}$ values (*see* Fig. 7) are relatively large and hence $\frac{dpa}{dZ}$ is relatively large. In zones B and D, on the other hand, $\frac{dh}{dZ}$ values are relatively small, and $\frac{dpa}{dZ}$ is also relatively small. Because the changes of q and μ in this case are quite gradual, a large $\frac{dpa}{dZ}$ will produce a small k value in equation (50) and vice versa. Low $\frac{dh}{dZ}$ values (B and D) are, therefore, associated with high average permeabilities. In zones of B and D, the shales have a higher permeability than those in A, C, and E, or some intercalation of such permeable rocks as sandstones and carbonate rocks may exist in B and D. In any event, the shale porosity distribution can be used as an instant indicator of the average permeability of rocks.

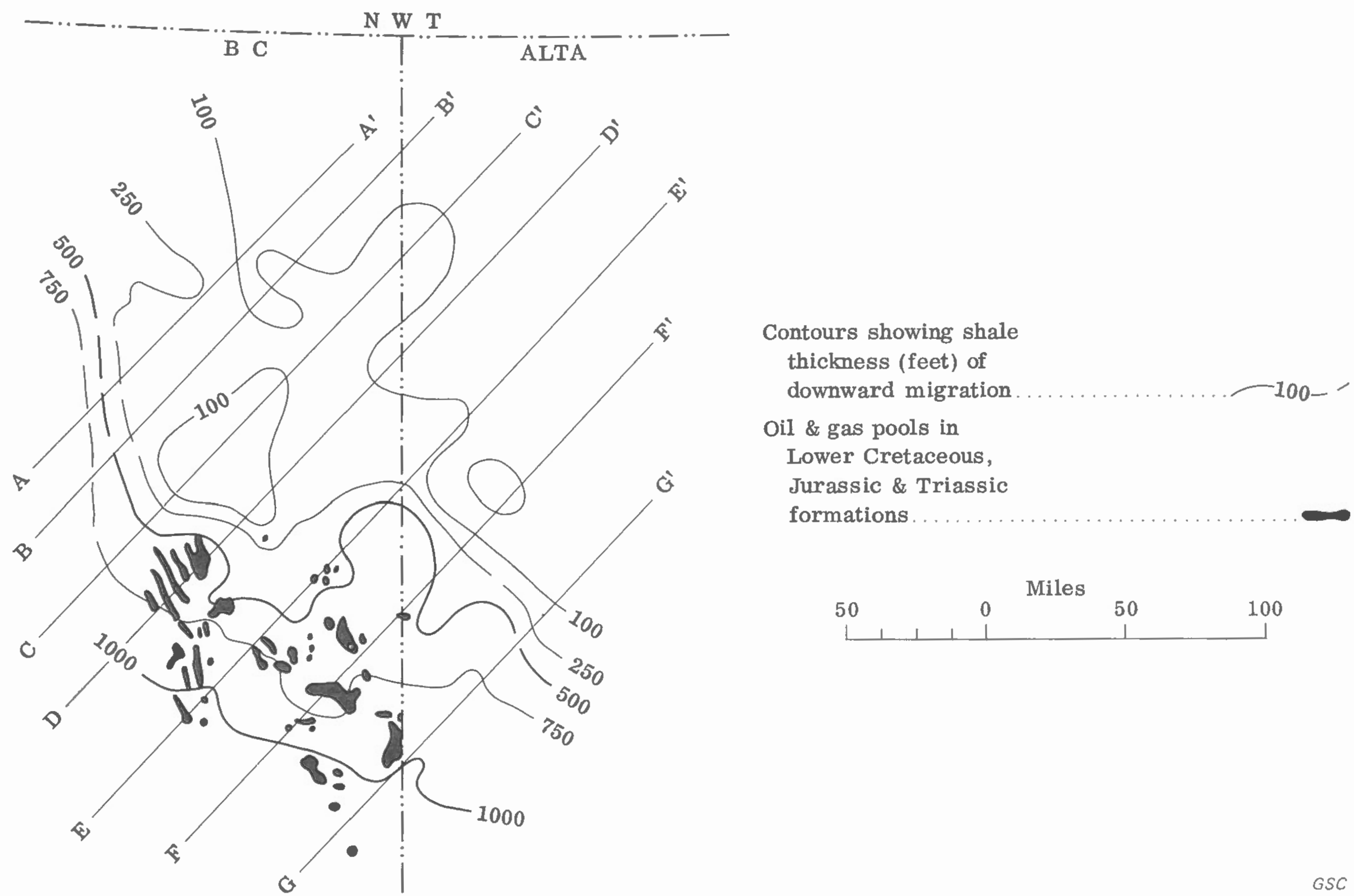

Figure 29. Contours showing thickness of downward migration zone

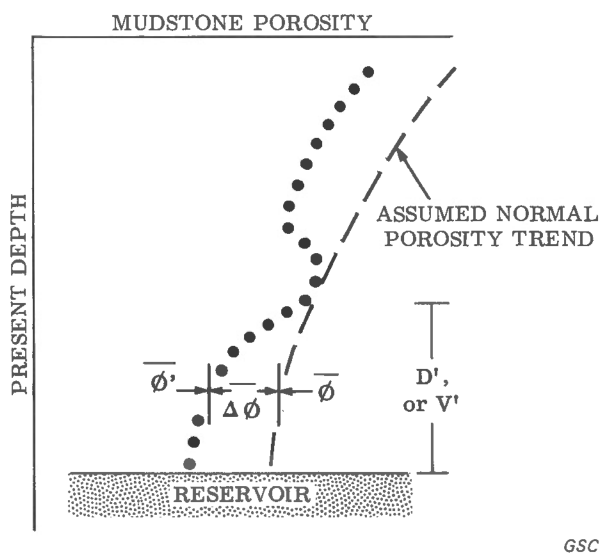

Figure 30. Schematic diagram showing shale porosity difference before and after compaction

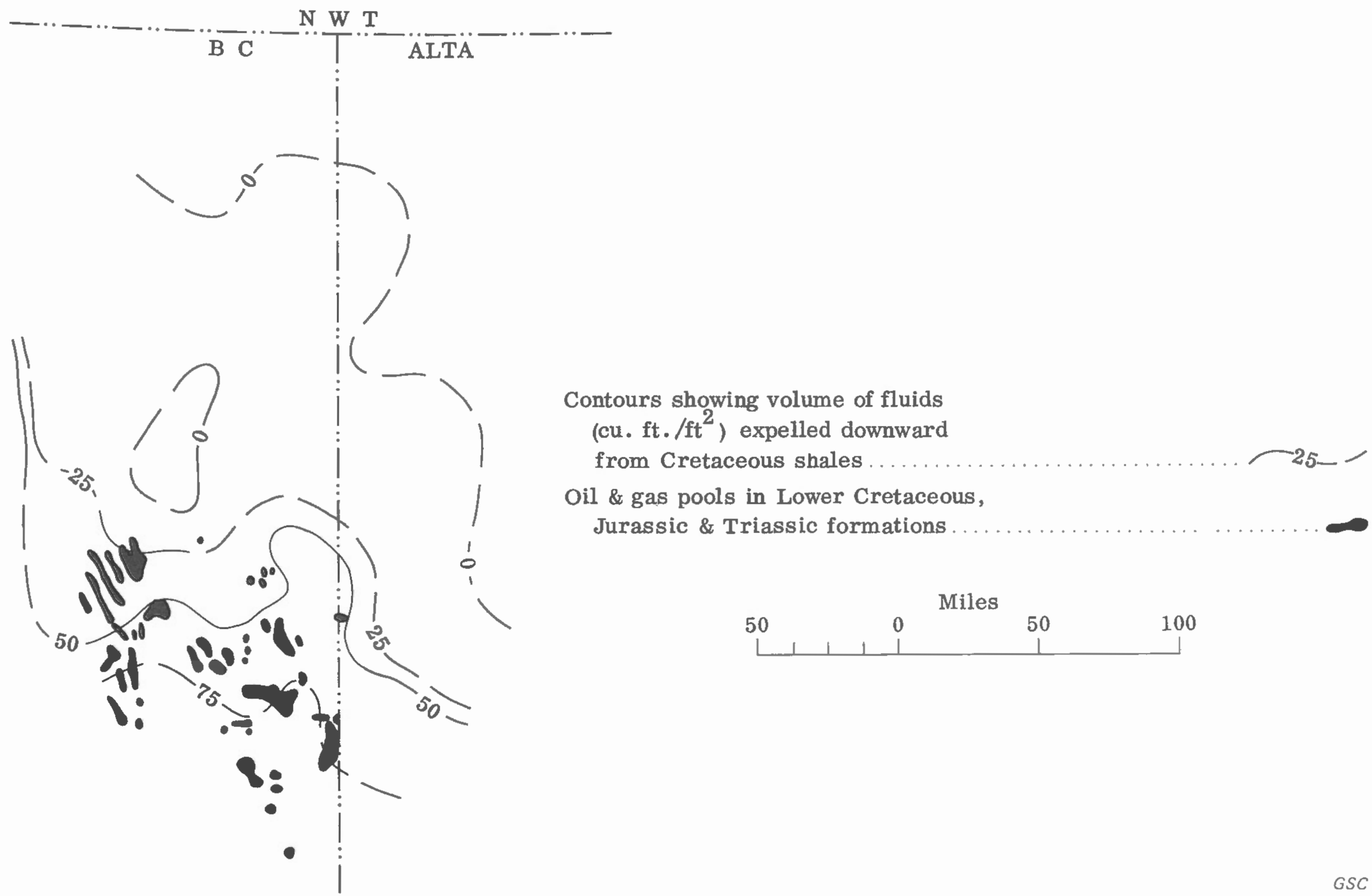

Figure 31. Volume of fluids expelled downward from shale

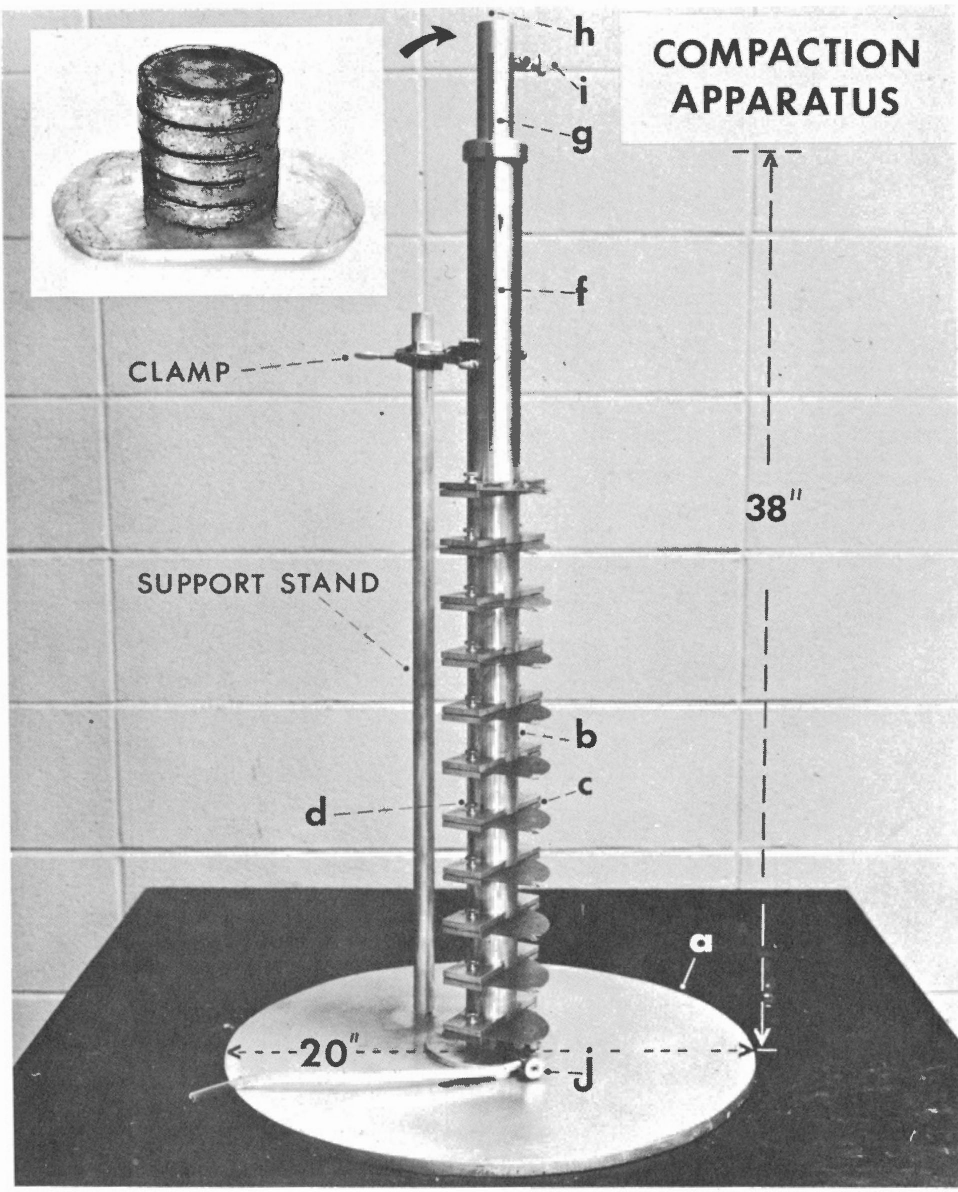

Figure 32. Compaction apparatus used for experiments

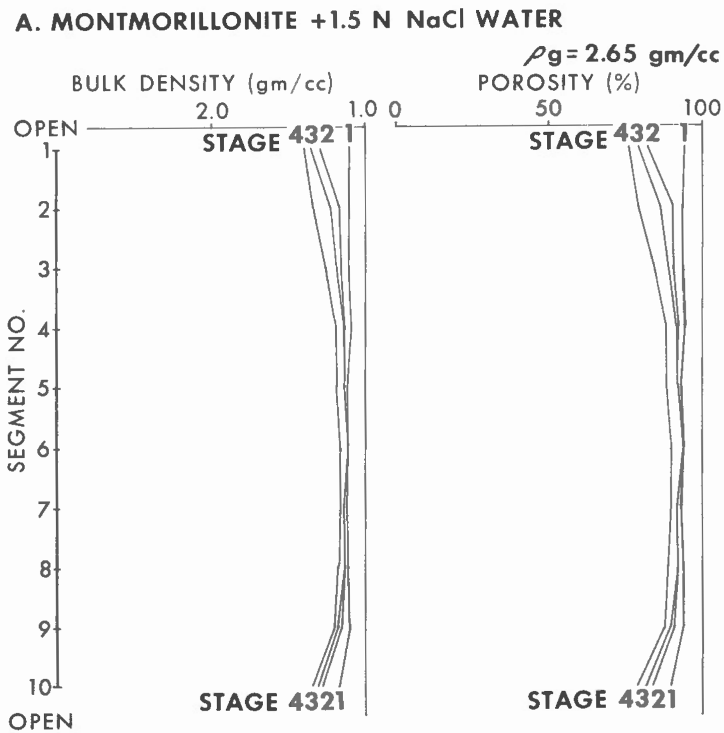

Figure 33. Chart showing bulk density and porosity at different stages of compaction experiment

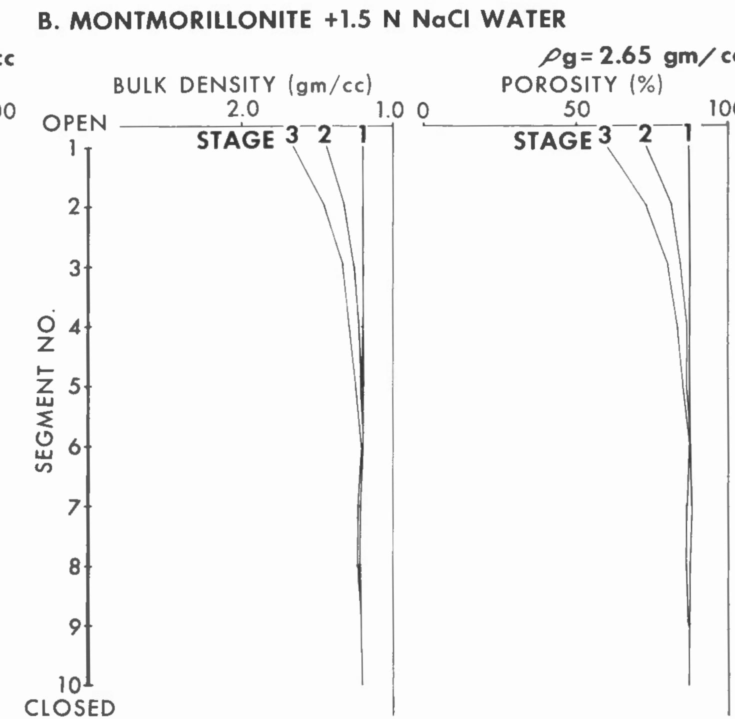

Figure 34. Chart showing bulk density and porosity at different stages of compaction experiment

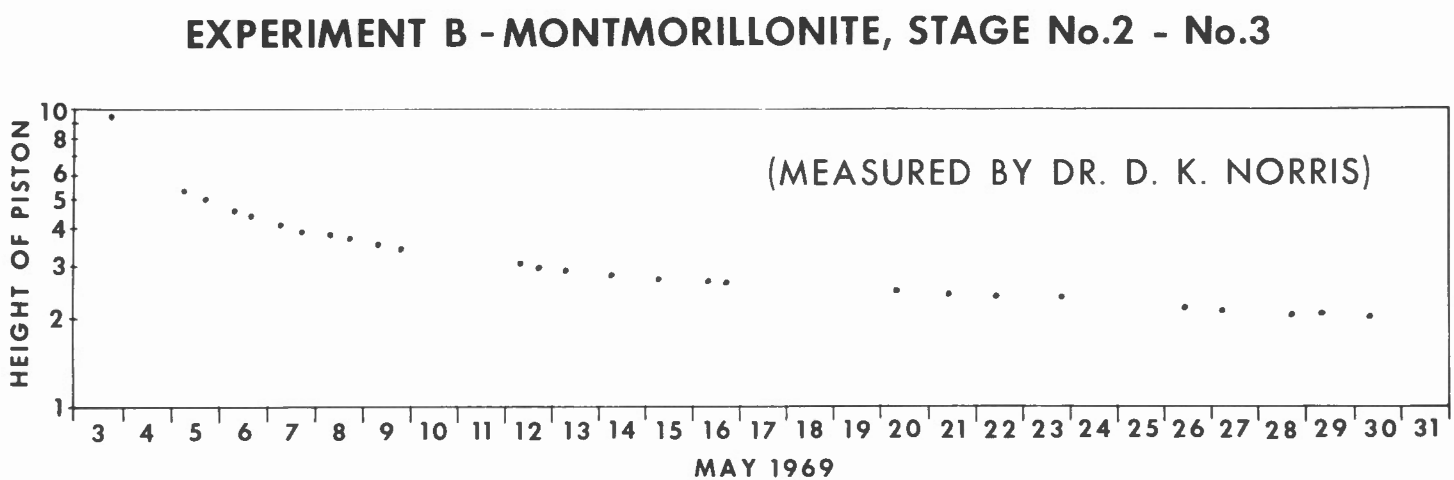

Figure 35. Diagram showing change of piston height with time

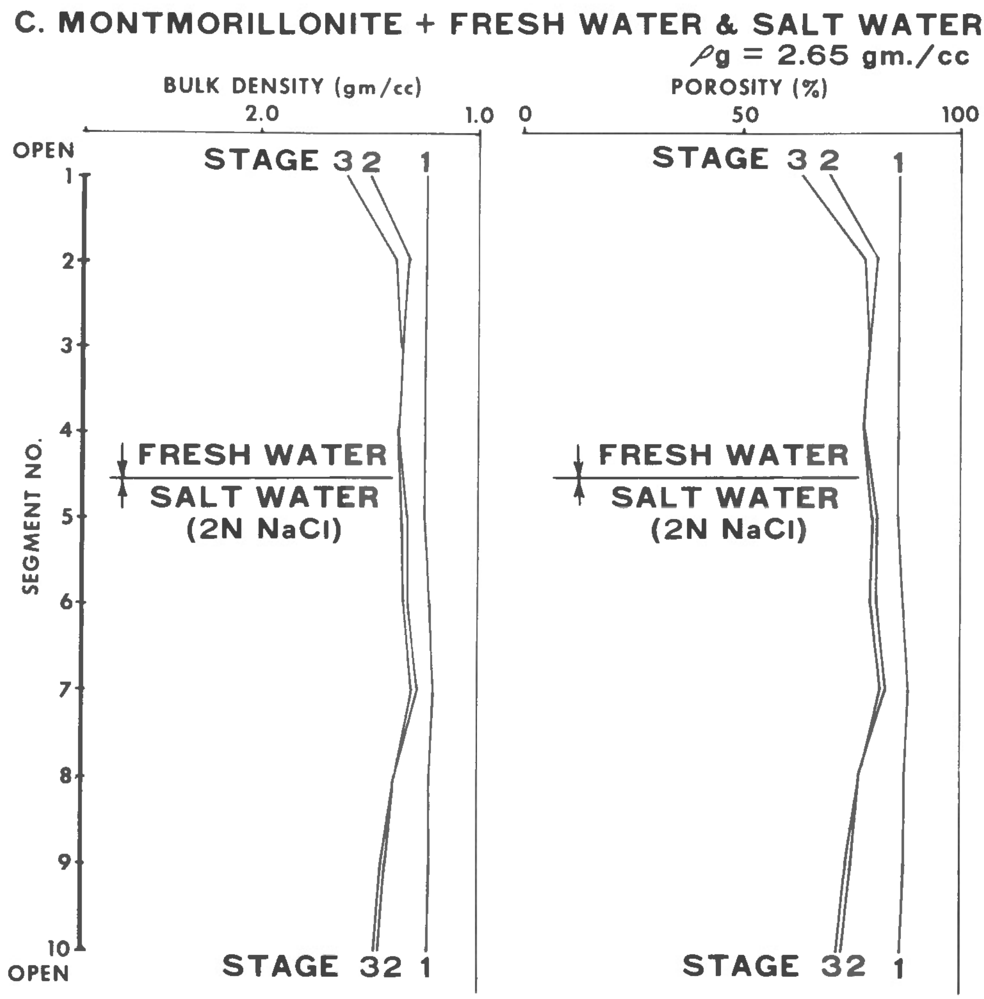

Figure 36. Chart showing bulk density and porosity at different stages of compaction experiment

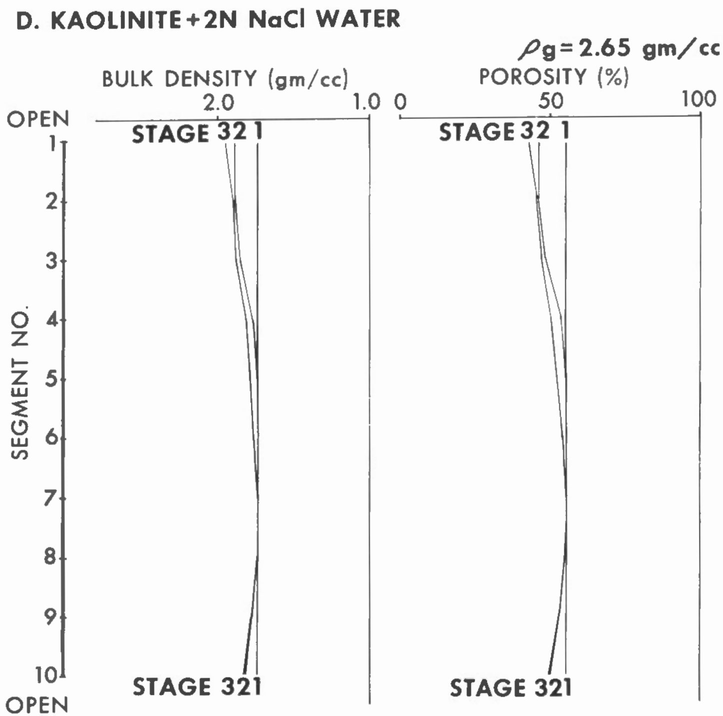

Figure 37. Chart showing bulk density and porosity at different stages of compaction experiment

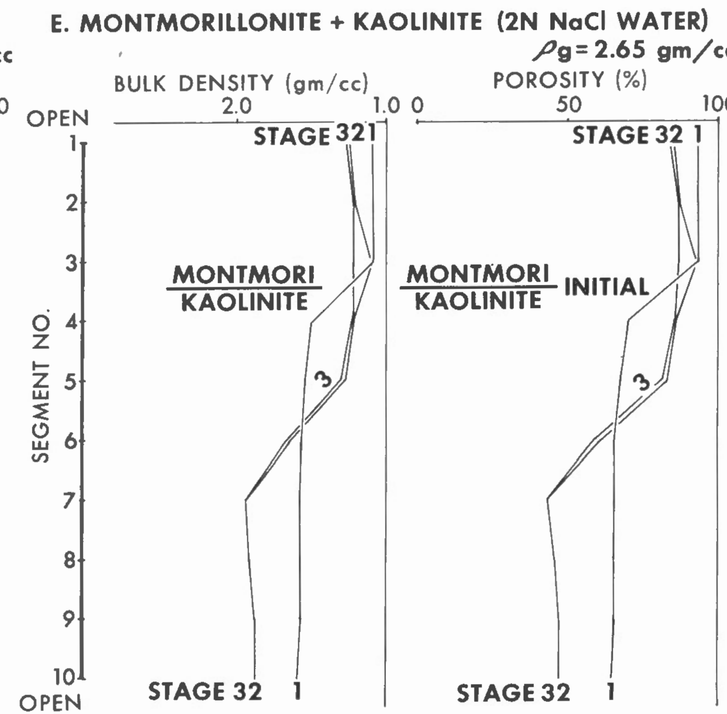

Figure 38. Chart showing bulk density and porosity at different stages of compaction experiment

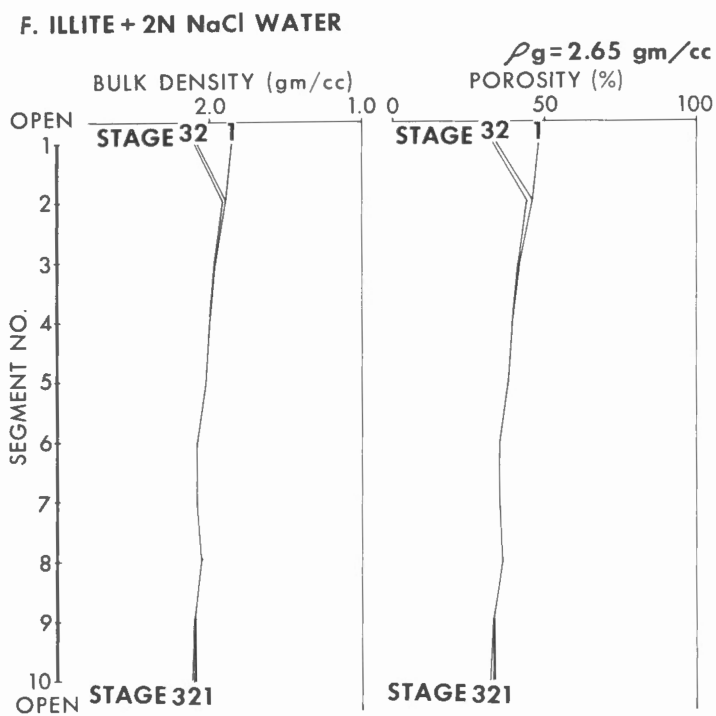

Figure 39. Chart showing bulk density and porosity at different stages of compaction experiment

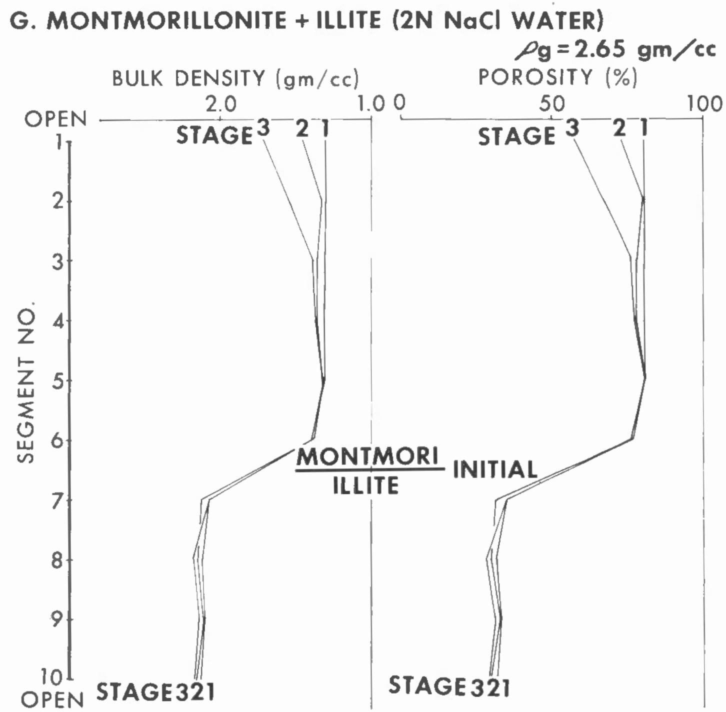

Figure 40. Chart showing bulk density and porosity at different stages of compaction experiment

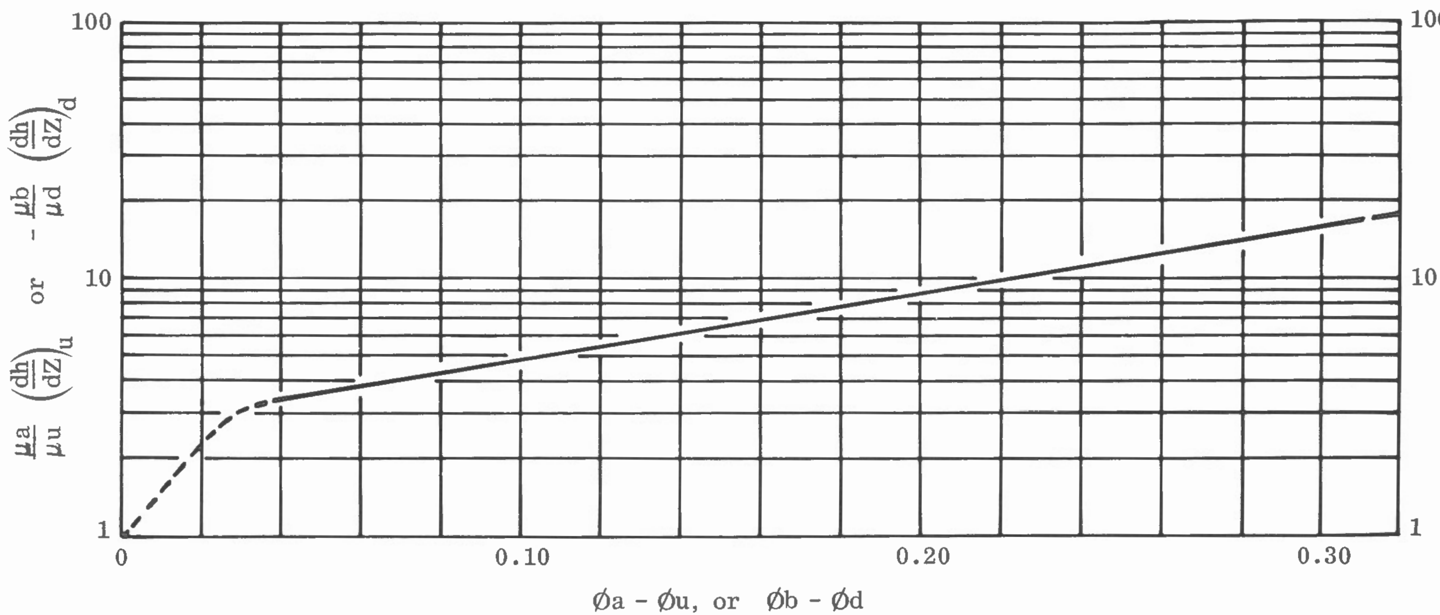

Figure 41. Chart showing the relationship between $\frac{\mu a}{\mu u}\left(\frac{db}{dZ}\right)_u$ and Øa - Øu or between $-\frac{\mu b}{\mu d}\left(\frac{dh}{dZ}\right)_d$ and Øb - Ød

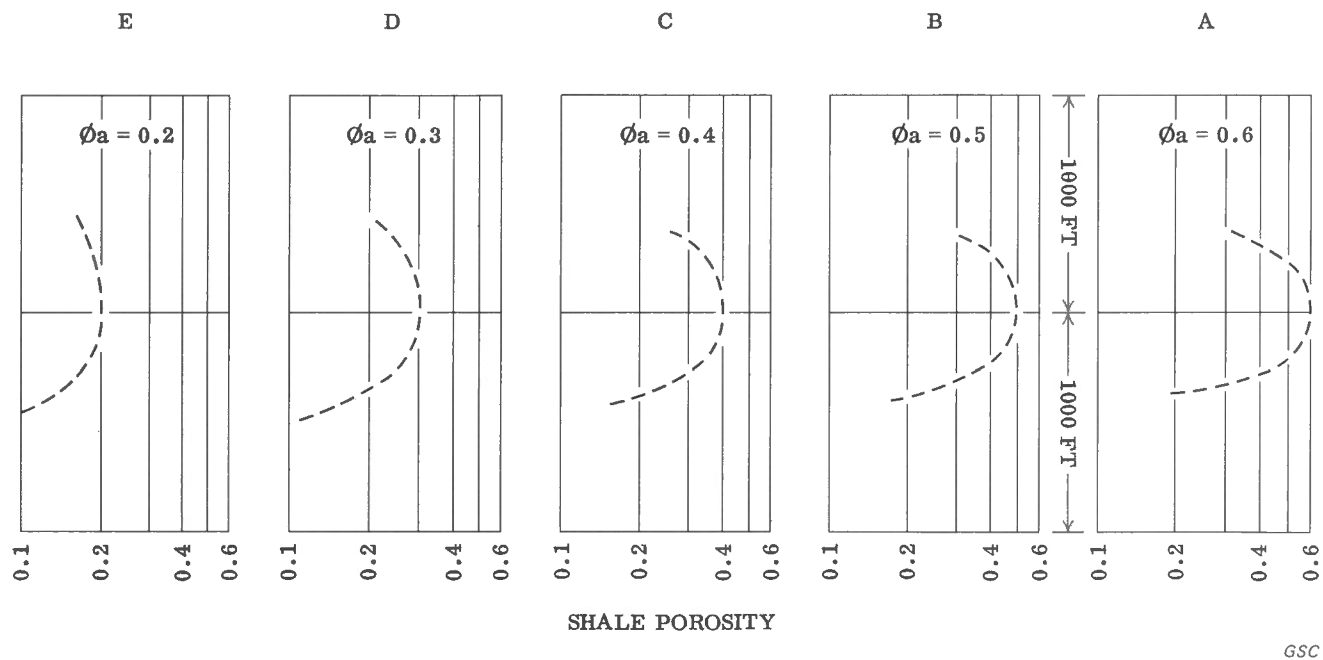

Figure 42. Chart showing porosity distributions of incompletely compacted shales

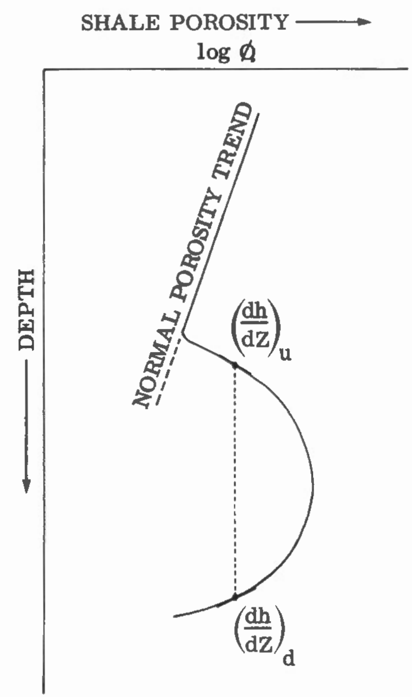

Figure 43. Schematic diagram showing the relationship between $\left(\frac{dh}{dZ}\right)_u$ and $\left(\frac{dh}{dZ}\right)_d$

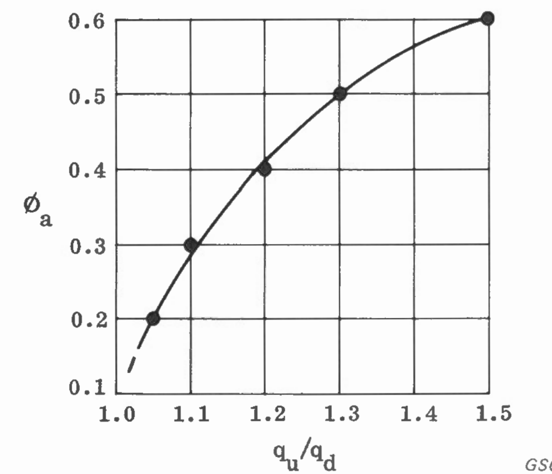

Figure 44. Relationship between ϕ_a and average value of q_u/q_d, based on constructed porosity distributions shown in Fig. 42

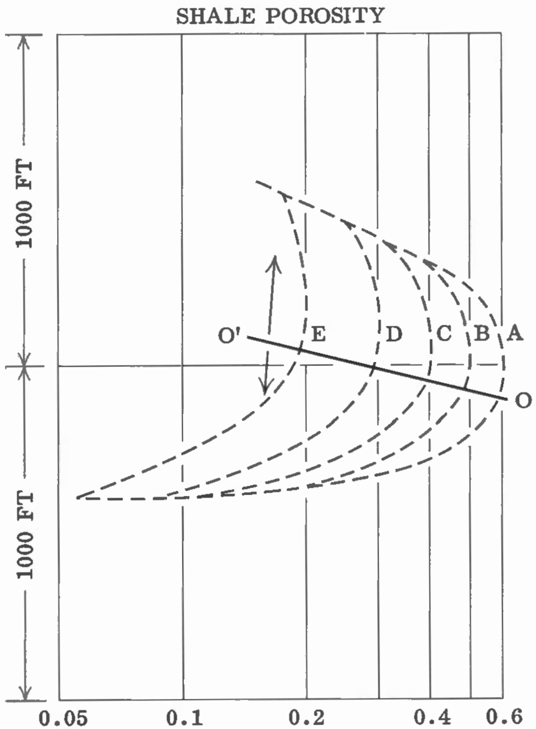

STAGES	AMOUNT OF WATER EXPULSION per ft.^{2}	
	UPWARD	DOWNWARD
A - B	30 ft.^{3}	22 ft.^{3}
B - C	31	25
C - D	33	29
D - E	40	37

STAGE A: $\phi a = 0.6$
B: $\phi a = 0.5$
C: $\phi a = 0.4$
D: $\phi a = 0.3$
E: $\phi a = 0.2$

GSC

Figure 45. Patterns of shale porosity distribution and amount of water expulsion from shales at several stages of compaction

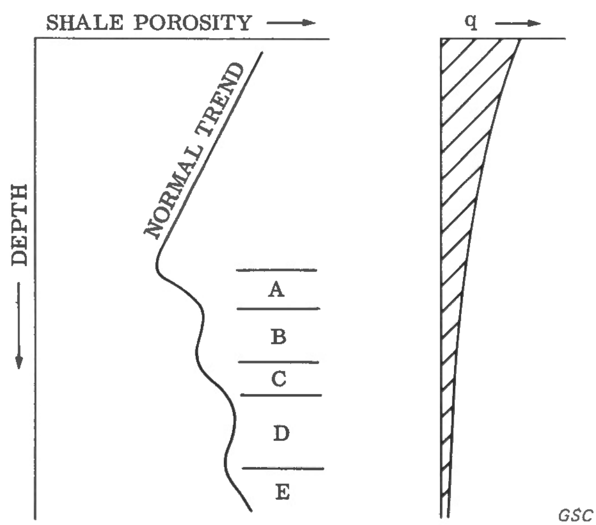

Figure 46. Schematic diagram showing shale porosity distribution as a permeability indicator

REFERENCES

Archie, G.E.
1942: The electrical resistivity log as an aid in determining some reservoir characteristics: Am. Inst. Mining Met. Eng. Trans., vol. 146, pp. 54-62.

1950: Introduction to petrophysics of reservoir rocks: Bull. Am. Assoc. Petrol. Geologists, vol. 34, No. 5, pp. 943-961.

Athy, L.F.
1930: Density, porosity, and compaction of sedimentary rocks: Bull. Am. Assoc. Petrol. Geologists, vol. 14, No. 1, pp. 1-24.

Bredehoeft, J.D. and Hanshaw, B.B.
1968: On the maintenance of anomalous fluid pressures: I, thick sedimentary sequence: Bull. Geol. Soc. Am., vol. 79, No. 9, pp. 1097-1106.

Burst, J.F.
1969: Diagenesis of Gulf Coast clayey sediments and its possible relation to petroleum migration: Bull. Am. Assoc. Petrol. Geologists, vol. 53, No. 1, pp. 73-93.

Chilingar, G.V. and Knight, L.
1960: Relationship between pressure and moisture content of kaolinite, illite and montmorillonite clays: Bull. Am. Assoc. Petrol. Geologists, vol. 44, No. 1, pp. 101-106.

Dickinson, G.
1953: Geological aspects of abnormal reservoir pressures in the Gulf Coast region of Louisiana, U.S.A.: 3rd World Petroleum Congress Proc., Sec. 1, pp. 1-16; 1953, Bull. Am. Assoc. Petrol. Geologists, vol. 37, No. 2, pp. 410-432.

Engelhardt, W. von, and Gaida, K.H.
1963: Concentration changes of pore solutions during the compaction of clay sediments: J. Sediment. Petrol. vol. 33, pp. 919-930.

Fons, L. and Holt, O.
1966: Formation log pressure data can improve drilling: World Oil, vol. 163, No. 4, pp. 70-74.

Foster, J.B. and Whalen, H.E.
1966: Estimation of formation pressures from electrical surveys - offshore Louisiana: J. Petrol. Technol., vol. 18, No. 2, pp. 165-171.

Hanshaw, B.B. and Bredehoeft, J.D.
1968: On the maintenance of anomalous fluid pressures: II, source layer at depth: Bull. Geol. Soc. Am., vol. 79, No. 9, pp. 1107-1122.

Hedberg, H.D.
1936: Gravitational compaction of clays and shales: Am. J. Sci., vol. 31, No. 4, pp. 241-287.

Hottmann, C.E. and Johnson, R.K.
1965: Estimation of formation pressures from log-derived shale properties: J. Petrol. Technol., vol. 17, No. 6, pp. 717-722.

Hubbert, M.K.
1953: Entrapment of petroleum under hydrodynamic conditions: Bull. Am. Assoc. Petrol. Geologists, vol. 37, No. 8, pp. 1954-2026.

Hubbert, M.K. and Rubey, W.W.
1959: Role of fluid pressure in mechanics of overthrust faulting, I, Bull. Geol. Soc. Am., vol. 70, No. 2, pp. 115-166.

Kok, P.C. and Thomeer, J.H.M.A.
1955: Abnormal pressures in oil and gas reservoirs: Geol. Mijnbouw, Aug.

Levorsen, A.I.
1954: Geology of petroleum: San Francisco, W.H. Freeman Co., 703 pp.

MacGregor, J.R.
1965: Quantitative determination of reservoir pressures from conductivity log: Bull. Am. Assoc. Petrol. Geologists, vol. 49, No. 9, pp. 1502-1511.

Magara, K.
1968a: Compaction and migration of fluids in Miocene mudstone, Nagaoka Plain, Japan: Bull. Am. Assoc. Petrol. Geologists, vol. 52, No. 12, pp. 2466-2501.

1968b: Subsurface fluid pressure profile, Nagaoka Plain, Japan: Bull. Japan Petrol. Inst., vol. 10, pp. 1-7.

Meade, R.H.
1966: Factors influencing the early stages of the compaction of clays and sands: Review, J. Sediment. Petrol., vol. 36, pp. 1085-1101.

Oil and Gas Conservation Board
1967: Pressure-depth and temperature-depth relationships, Alberta crude oil pools, OGCB-67-22, Calgary, Alberta.

Pirson, S.J.
1963: Handbook of well log analysis: N.J., Prentiss-Hall, Englewood Cliffs.

Powers, M.C.
1967: Fluid-release mechanisms in compacting marine mud-rocks and their importance in oil exploration: Bull. Am. Assoc. Petrol. Geologists, vol. 51, pp. 1240-1253.

Rogers, L.C.
1966: How Shell controls Gulf Coast pressures: Oil and Gas J.. vol. 64, No. 20, pp. 264-266.

Rubey, W.W. and Hubbert, M.K.
1959: Role of fluid pressure in mechanics of overthrust faulting, II, Bull. Geol. Soc. Am., vol. 70, pp. 167-206.

Thomeer, J.H.M.A. and Bottema, J.A.
1961: Increasing occurrence of abnormally high reservoir pressures in boreholes, and drilling problems resulting therefrom: Bull. Am. Assoc. Petrol. Geologists, vol. 45, No. 10, pp. 1721-1730.

Wallace, W.E.
1965: Abnormal subsurface pressures measured from conductivity or resistivity logs: Oil and Gas J., vol. 63, No. 27, pp. 102, 104-106.

Weller, J.M.
1959: Compaction of sediments, Bull. Am. Assoc., Petrol. Geologists, vol. 43, No. 2, pp. 273-310.

Wyllie, M.R.J., Gregory, A.R. and Gardner, L.W.
1956: Elastic wave velocities in heterogeneous and porous media: Geophysics, vol. 21, No. 1, pp. 41-70.

Wyllie, M.R.J., Gregory, A.R. and Gardner, G.H.F.
1958: An experimental investigation of factors affecting elastic wave velocities in porous media: Geophysics, vol. 23, pp. 459-493.

APPENDIX

(Tables 1-5)

TABLE 1

LIST OF WELLS USED FOR DETERMINATION OF POROSITY - Δt RELATIONSHIP OF SHALES	
Well	Location
Imp. Avon Hill	12-15V- 30-22-W3
Amerada Cdn. Sup. Ferrier	10- 7 - 41- 8-W5
I.O.E. Galaxy	10- 8 -110- 5-W6
B.A. Calling Lake	6-36 - 71-23-W4
N.C.O. Richmond (Sonic only)	6-29 - 18-27-W3
N.C.O. Richmond (Density only)	11-10 - 18-27-W3
Pan Am A-1 Algar River	4-13 - 87-17-W4
Mule Creek Yorkton	14-28 - 27- 3-W2
Pan Am D_1 Chipewyan	10-16 - 91-18-W4
Texaco I.O.E. Buffalo	10-15 - 85-22-W4
Pan Am A-1 Frog Lake	10-29 - 58- 2-W4
Dome Provo Zama N	10-14 -117- 4-W6
B.A. Zama North	2-16 -117- 4-W6
B.A. H.B. Zama North	5-30 -116- 4-W6

TABLE 2

LIST OF WELLS STUDIED			
Group	Well No.	Well Name	Location
A.	1.	I.O.E. Pan Am Boundary	14 -21 -84-13W6
	2.	C.& E. Pacific Doe Creek	6 -10 -82-13W6
	3.	I.O.E. et al. Clear River	10 - 5 -84-11W6
	4.	T.P.C.& O. et al. Clear River	10 -30 -83-11W6
	5.	T.P.C.& O. et al. Clear River	14 -21 -84-10W6
	6.	Altair H.B. Josck	7 -24 -82-10W6
	7.	C.D.R. Royce	2 -12 -83- 8W6
B.	8.	I.O.E. Peace Grove	10 -16 -84- 5W6
	9.	Union et al. Dunvegan	7 -13 -81- 5W6
	10.	Amerada Crown C.D. Bingo	5 -35 -82- 3W6
	11.	Samedan Decalta Berwyn	2 -36 -82-25W5
C.	12.	K.C.L. Tenn Roma	10 -36 -83-23W5
	13.	Garvey et al. Cadotte	6 -36 -85-19W5
	14.	Shell Peace River	13 -25 -83-17W5
	15.	Can. Delhi et al. Cadotte	5 -32 -83-16W5
	16.	Imp. et al. Heart R.N.	2 - 9 -83-15W5
D.	17.	H.B. Union Lubican	10 -24 -86-13W5
	18.	R.O. Corp. et al. E. Lubican	4 -32 -83-12W5
	19.	Texaco Pan Am Lubican S.	2 -32 -83-11W5
	20.	I.O.E. Chevron Lubican River	2 -27G1-84-10W5
	21.	I.O.E. B.A. Loon Lk. S.	12 -15 -85- 9W5
	22.	I.O.E. Bat Lake	15 - 8 -84- 8W5

TABLE 3

MUDSTONE POROSITY AND PERMEABILITY DATA
OF WELL CORES IN JAPAN & CANADA

Well	Depth	Lithology	Permeability (md)	Porosity	Permeant
Obuchi stratigraphic well (Japan)	1454 m	Mudstone	9.9×10^{-3}	0.257	8,000 mg/1 NaCl solution
	2036	do	1.2×10^{-2}	0.203	
	2488	do	1.0×10^{-2}	0.150	
	3049	do	9.1×10^{-3}	0.127	
	3053	do	8.6×10^{-3}	0.152	
	4033	do	0	0.065	
Kambara GS-1 (Japan)	1029 m	Mudstone	-	0.390	
	1609	do	-	0.332	
	1808	do	7.7×10^{-3}	0.266	10,000 ppm NaCl solution
	2005	do	9.9×10^{-3}	0.311	
	2151	Sandy Mudstone	3.0×10^{-2}	0.246	
	2295	Mudstone	7.3×10^{-3}	0.243	
	2608	do	1.0×10^{-3}	0.218	
	3062	do	2.6×10^{-3}	0.196	
	3206	do	2.0×10^{-4}	0.188	
	3503	do	1.3×10^{-3}	0.159	
	3701	do	8.0×10^{-4}	0.146	
Kambara GS-2 (Japan)	1000 m	Siltstone	4.9×10^{-2}	0.399	10,000 ppm NaCl solution
	1255	Mudstone	1.4×10^{-2}	0.427	
	1501	Sandy Mudstone	1.4×10^{-2}	0.377	
	1763	Mudstone	2.3×10^{-2}	0.294	
	2508	do	6.0×10^{-3}	0.246	
	3500	do	7.0×10^{-3}	0.122	
	4103	Sandy Mudstone	8.0×10^{-3}	0.080	
Yuza GS-1 (Japan)	807 m	Siltstone	2.1×10^{-2}	0.427	8,000 mg/1 NaCl solution
	1008	do	2.4×10^{-3}	0.382	
	1198	Mudstone	8.4×10^{-3}	-	
	1398	do	1.2×10^{-3}	0.241	22,000 gm/1 NaCl solution
	1614	do	1.3×10^{-3}	0.187	
	1966	do	1.0×10^{-3}	0.163	
	2201	do	6.0×10^{-4}	0.161	
	2402	do	5.0×10^{-4}	0.153	
	2586	do	4.0×10^{-4}	0.164	14,000 mg/1
	2816	do	1.0×10^{-4}	0.180	
Strathmore 7-12-25-25W4	770 ft	Shale	1.6×10^{-4}	0.195	32,000 ppm NaCl solution
	777	do	1.0×10^{-6}	0.205	

Group	Well No.	Well Name	Location
E.	23.	Uno-Tex Red E.	4 - 3 -87- 8W5
		Uno-Tex Red E.	12 - 4 -87- 8W5
	24.	Uno-Tex B.A. Red E.	11 -33 -86- 8W5
	25.	Home et al. Red Earth	4 -16 -87- 7W5
	26.	B.A. Pastecho River	2 -30 -79- 4W5
	27.	I.O.E. Trout River	10 -30 -83- 3W5
	28.	Pan Am A-1 Doucette	7 -28 -78- 2W5
F.	29.	I.O.E. Corn Lake	4 - 3 -88-25W4
	30.	I.O.E. Buffalo River	4 -32 -85-23W4
	31.	Sun Pan Am Wabasca	10 - 5 -83-21W4
	32.	C.N.D.-S.U.P. Mink	10 -16 -90-20W4
	33.	Pan Am B-1 Chipewyan	8 -32 -91-19W4
		Pan Am 2 Chip Strat	8 -35 -91-19W4
	34.	Pan Am D1 Chipewyan	10 -16 -91-18W4
		Pan Am E1 Chipewyan	10 -34 -91-18W4
	35.	Champlin Pa McKay	10 -32 -88-15W4
G.	36.	Amerada C.D.N.-S.U.P. Brewster	4 -26 -42-11W5
	37.	Dekalf Crimson	7 -36 -42-10W5
	38.	Amerada C.D.N.-S.U.P. Crimson	12 -29 -42- 9W5
	39.	Amerada C.D.N.-S.U.P. Ferrier	10 - 7 -41- 8W5
	40.	Amerada Crown	CG6 - 5 -42- 7W5
	41.	Amerada Crown Cy. Will. Gr.	6 -21 -41- 7W5
		Willcan Will. Gr.	6 -36 -41- 7W5
H.	42.	Amerada Crown D.J. Minhik	7 -23 -45- 6W5
	43.	Climax Will. Gr.	16 -16 -42- 6W5
	44.	Apache Placid Carl Gilby	4 -35 -41- 5W5
		Apache Placid Carlos	12 -35 -41- 5W5
	45.	G.R.T. P.L.N.S. Minhik	6 - 4 -46- 5W5
	46.	Tenn Marathon A1 Pendryl	10 -16 -46- 4W5
	47.	Skelly A-1 Pendryl	12 - 6 -45- 4W5
	48.	Calstan Wenham	4 -34 -46- 3W5
	49.	Joe Phillips Wrose S.	1 - 4 -45- 1W5
I.	50.	Forgotson-Burk Sgspike	15 -33 -50-27W4
	51.	S.O.B.C. Imp. Leduc	10 -11 -50-26W4
	52.	Midwest et al. Blackmud	8 - 7 -51-24W4
	53.	N.U.L. Oliver	10 - 4 -54-23W4
	54.	N.U.L. Fort Saskatchewan	10 -33 -54-22W4
	55.	Ashiand Amax Ardrossan	12 -34 -52-22W4
	56.	S.O.B.C. C.S. Camrose West	10 - 3 -50-22W4
J.	57.	H.H.S.-C.P.O.G. Tawayik	12 - 9 -53-19W4
		C.P.O.G. Chipman	10 -22 -53-19W4
	58.	N.U.L. Beaverhill Lake	10 -27 -52-19W4
	59.	Canso et al. Lamont	10 -25 -55-18W4
	60.	C.P.O.G. Chipman	10 - 2 -53-18W4
	61.	C.P.O.G. Dusty Lake	11 -12 -48-18W4
	62.	Altair Lloyd Hilliard	1 - 5 -54-17W4
	63.	H.L. Hunt Mundare	12 -11 -53-17W4
K.	64.	Scurry Hairy Hill	10 -24 -55-14W4
	65.	Canpet Mont Imp. Ispas	4 -26 -57-13W4
	66.	B.A. Spedden	11 -23 -59-12W4
	67.	Sun Imp. Lottie	10 - 2 -59-11W4

Group	Well No.	Well Name	Location
L.	68.	B.A. Mallaig	7 -26 -60-10W4
	69.	Triad Dev-Pal Therien	7 -25 -60- 9W4
	70.	Imp. Lac. Canard	12 -10 -57- 9W4
	71.	Triad Dev-Pal Glendon	11 -31 -60- 7W4
	72.	Triad Dev-Pal Kehiwin	10 -34 -59- 7W4
M.	73.	Cansalt Linbergh	6 -10 -58- 5W4
		Cansalt Linbergh	4 -18 -58- 5W4
	74.	Pan Am A-1 Muriel Lake	10 - 5 -59- 4W4
	75.	Imp. Beaverdam	5 -16 -60- 2W4
	76.	Pan Am A-1 Frog Lake	10 -29 -58- 2W4
	77.	Husky Blackfoot Lloyd	10A- 2 -50- 2W4
	78.	B.A. Sputinow	13C- 3 -58- 1W4
		B.A. Sputinow	16A-27 -58- 1W4
N.	79.	Imp. Beaver River	14 -23 -60-27W3
	80.	Imp. Worthington	8 -28 -58-27W3
	81.	Imp. Cold Lake East No. 1	6 -23 -64-26W3
	82.	Imp. Ministikwan	9 - 3 -59-26W3
	83.	Imp. Oldman Lake	2 - 9 -54-26W3
	84.	Imp. Northern Pine	16 -16 -63-25W3
	85.	Cigol Amerada Watson Lake	10 - 5 -60-22W3
O.	86.	C.P.O.G. Milk River Ridge	10 -12 - 4-20W4
	87.	Uno-Tex. H.B. Iron Springs	10 -36 -10-20W4
	88.	C.P.O.G. New Dayton	5 -30 - 4-18W4
	89.	L.-M. Turin	6 -34 -10-18W4
	90.	C.P.O.G. Taber	11 -26 - 9-17W4
	91.	Barons C.P.O.G. Taber North	4 -33 -10-16W4
	92.	Loc. et al. Tabern	2 - 5 -11-16W4
P.	93.	C. and E. Fincastle	15 -17 -10-15W4
	94.	Gridoil Hays	2 - 9 -13-13W4
	95.	C.P.O.G. Tilley	2 -27 -16-13W4
	96.	Empire St. et al. Bantry E.	4 - 3 -17-12W4
	97.	Gridoil Bow Island Burdett 1	4 - 8 -11-11W4
	98.	Gridoil C.F. Illingworth	10 -10 -13-11W4
		B.A. Grand Forks	10 -21 -13-11W4
	99.	Calstan C.P.R. Kininvie	4 -17 -17-11W4
		Suptst et al. Monogam	12 -28 -17-11W4
Q.	100.	Kerr McGee Princess	10 -24 -20-10W4
	101.	Home et al. Suffield	3 -27 -13- 9W4
	102.	R.O. Corp. Monogram	10 -29 -16- 9W4
	103.	Empire St. et al. Jenner	10 -27 -19- 9W4
	104.	Empress Suffield	10 - 5 -14- 8W4
	105.	Empire St. et al. Jenner	4 -33 -20- 8W4
	106.	Pembina Midcon. Med. Hat	6 -25 -13- 6W4
	107.	Dev.-Pal. P.O.R. Acadia	6 - 2 -24- 4W4
	108.	Baysel et al. Bindloss	10 -32 -20- 2W4
R.	109.	N.C.O. Richmond	6 -29 -18-27W3
	110.	Husky Marengo	7 -29 -27-27W3
	111.	Oliphant N.W. Gorefield	10 -18 -24-26W3
	112.	Imp. Bayhurst	7 -22 -24-25W3
	113.	C.D.R.S. Sceptre	2 - 3 -21-24W3
	114.	Continental Avon Hill Dodsland	10 -31 -30-22W3
		Imp. Avon Hill	12 -15V-30-22W3
	115.	Williamson Shackleton	2 -21 -18-20W3

Group	Well No.	Well Name	Location
S.	116.	Kissinger Rancho Herschel	13-17-30-17W3
	117.	Rothwell Socony Matador	1-15-21-15W3
	118.	Imp. Rossduff	4- 2-24-10W3
	119.	H.B. Mobil Log Valley	16- 4-20- 8W3
	120.	H.B. Sunkist	12-18-21- 8W3
	121.	C.D.R. Eyebrow	4-15-21- 2W3
	122.	Sifto Salt (1960) Tugaske	4-10-23- 2W3
		Placid Sifto Tugaske	2-10-23- 2W3
T.	123.	Placid Allen	4-29-32-28W2
	124.	Porcupine Prime Imp.	8-28-27-26W2
	125.	Alwinsal Mohawk	1-10-33-24W2
	126.	Scurry Boulder Lake	1-24-30-23W2
	127.	K.R. Nokomis	16- 2-30-21W2
U.	128.	N.P.C. Touchwood	1-18-31-18W2
	129.	Miami H.B. Quill Lake	13-22-30-16W2
	130.	Atlantic Raymore	16- 6-29-15W2
	131.	Scurry Foam Lake	5-31-30-12W2
V.	132.	Shell Insinger	5-28-29- 9W2
	133.	B.A. Invermay	1-29-31- 7W2
	134.	Mule Crk. Yorkton	14-28-27- 3W2
W.	26.	B.A. Pastecho River	2-30-79- 4W5
	28.	Pan Am. A-1 Doucette	7-28-78- 2W5
	135.	Pan Am. G-1 Marten Hills	6-32-75- 1W5
	136.	B.A. Calling Lake	6-36-71-23W4
	137.	Champlin Flat Lake	11-35-65-20W4
	138.	Tenn C. and E. Flat Lake	1-31-65-19W4
	139.	C.P.O.G. Perryvale	11-20-63-21W4
X.	140.	C.P.O.G. Viking	10-29-45-10W4
	141.	Home et al. Hardisty	10-30-42- 9W4
	142.	C.P.O.G. Kess	10- 9-40- 8W4
	143.	Mobil C.P.O.G. Brownfield	11-15-38-12W4
	144.	Dynamic et al. Provost	10-30-35- 3W4
	145.	B.A. Royalite Calthorpe	10-16-32- 1W4
	146.	Mobil Oyen	10- 4-30- 2W4
Y.	147.	S.M.P.S. Gull Lake	3- 7-13-18W3
	148.	Texaco Scotsguard	2-32-10-16W3
	149.	Amax et al. Chamberry	4-17- 7-18W3
	150.	International Helium Wood Mountain	10- 3- 5- 8W3

TABLE 4

MINERAL IDENTIFICATION

STRATHMORE 7-12-25-25W4

(by A.E. Foscolos)

Depth (feet)	Order of Abundance
600	Montmorillonite, quartz, feldspar, illite, kaolinite.
700	Montmorillonite, quartz, feldspar, illite, kaolinite.
800	Montmorillonite, quartz, feldspar, illite, kaolinite.
820	Quartz, feldspar, montmorillonite, illite, kaolinite.
899	Quartz, montmorillonite, feldspar, illite, kaolinite.
998	Montmorillonite, quartz, feldspar, kaolinite and illite.
1100	Quartz, montmorillonite, feldspar, trace of kaolinite and illite.
1118	Quartz, feldspar, siderite, montmorillonite, kaolinite, trace of illite.
1200	Quartz, feldspar, kaolinite, montmorillonite, traces of illite and calcite.
1300	Quartz, feldspar, kaolinite, montmorillonite, trace of illite.
1378	Quartz, feldspar, montmorillonite, kaolinite, traces of illite, calcite and dolomite.
1425	Quartz, siderite, feldspar, traces of montmorillonite, kaolinite and illite.
1500	Quartz, feldspar, montmorillonite, kaolinite, illite, dolomite, siderite, traces of calcite and pyrite.
1600	Quartz, feldspar, kaolinite, montmorillonite, illite, pyrite and trace of calcite.
1700	Quartz, kaolinite, illite, feldspar, montmorillonite, trace of calcite, siderite and pyrite.
1740	Quartz, montmorillonite, feldspar, kaolinite, illite, pyrite and calcite.
1800	Quartz, montmorillonite, feldspar, kaolinite, trace of illite.
1900	Quartz, feldspar, montmorillonite, kaolinite, trace of illite, calcite, dolomite and siderite.
2000	Quartz, dolomite, illite, kaolinite, feldspar, calcite, trace of chlorite, siderite and pyrite.
2080	Quartz, dolomite, feldspar, illite, kaolinite, montmorillonite, calcite, traces of chlorite, siderite and pyrite.
2100	Quartz, montmorillonite, feldspar, kaolinite, illite, trace of calcite.
2200	Quartz, montmorillonite, feldspar, kaolinite, illite and trace of calcite.
2300	Quartz, feldspar, kaolinite, montmorillonite, illite, trace of calcite and dolomite.
2400	Quartz, feldspar, montmorillonite, kaolinite, illite and trace of calcite and dolomite.
2520	Quartz, feldspar, montmorillonite, kaolinite, illite and trace of calcite, dolomite and pyrite.

TABLE 5

LIST OF WELLS USED FOR DETAILED STUDY

A. Wells on Sections A-G	Location
C.D.R. Prophet	a- 61-J, 94-G-14
C.D.R. Pac. Sinc. Prophet	d- 21-B, 94-J-3
Pure Pac. Tenaka	c- 94-L, 94-J-2
Triad et al. Jackfish	c- 13-I, 94-J-7
P. Jackfish Triad Sohio	a- 30-K, 94-J-8
B.A. Shell Klua	b- 68-G, 94-J-9
B.A. Shell Klua	b- 49-F, 94-J-9
Clarke L.W. Nat. Imp.	b- 78-J, 94-J-9
Pac. Gunnel	b- 5-D, 94-I-13
Pac. Utahn	a- 83-C, 94-I-13
Placid Front Yoyo	d- 95-H, 94-I-13
W. Nat. et al. Yoyo	b- 29-I, 94-I-13
Kewanee Uno-Tex Yoyo	a- 49-L, 94-I-14
W. Nat. et al. Louise	d-100-E, 94-P-3
Atlantic Pac. E. Kotcho	b- 19-G, 94-P-3
Dome et al. Heimet	a- 59-J, 94-P-7
Williamson Pac. Bougie	d- 31-F, 94-G-15
Pure Imp. Bull.	b- 67-J, 94-J-1
Fina et al. Swat	a- 81-A, 94-J-8
Soc. Mobil Swat	b- 50-F, 94-I-5
Triad Uno-Tex Nogah	c- 78-H, 94-I-12
Mobil W. Sahtaneh	c- 89-I, 94-I-12
Soc. Mobil S. Sierra	a- 98-K, 94-I-11
Soc. Mobil Sierra	c- 78-C, 94-I-14
Kerr McGee et al. Sierra	a- 27-F, 94-I-14
S.O.B.C. Calstan. Peggo	b- 74-A, 94-P-7
Baysel N. Bistcho	12-25-123-7W6
Sinclair C.D.N. At. Calvan	d- 12-K, 94-G-2
Pan Am Dome Sikanni	b- 43-B, 94-G-7
Sinclair et al. Kahnta	b- 70-J, 94-G-7
Pan Am Dome Green	d- 76-I, 94-G-7
Pan Am Dome Medana	c- 26-H, 94-G-10
C.D.N. S.U.P. Fina Alum Trutch	a- 75-C, 94-G-16
Sinc. et al. N. Conroy Cr.	d- 45-K, 94-H-12
Amerada et al. Fontas	a- 61-K, 94-I-3
Texaco N.F.A. Townsoitoi	d- 44-C, 94-I-10
Sohio C. & E. Ekwan	a- 55-G, 94-I-10
Pac. Shekilie	b- 24-A, 94-I-16
Canso et al. Bistcho L.	10-27-119-6W6
Canso et al. Bistcho L.	12-20-122-4W6
Placid et al. E. Bistcho	5- 4-124-2W6
Tex. Texcan	d- 71-I, 94-B-15
Sinclair Pac. N. Julienne	c- 54-H, 94-G-2
Sinclair et al. Beg	b- 99-B, 94-G-1
Pac. Imp. S. Jedney	b- 09-H, 94-G-1
Pac. Sunray Imperial	b- 44-J, 94-G-1
Pac. Sunray Imp. Bubbles	d- 55-I, 94-G-1
Pac. I.O.E. Laprise	a- 85-D, 94-H-5
Pac. Imp. Laprise	a- 29-E, 94-H-5
Dome Prosper Martin Cr.	c- 18-H, 94-H-5
Tex. N.F.A. Black Cr.	c- 51-L, 94-H-6
Cigol Triad Conroy	a- 70-H, 94-H-12

Whiterose et al. Slave	b- 57-B, 94-H-14
Arco Pan. Am. Bedji	c- 32-E, 94-I-1
I.O.E. Teklo	c- 77-D, 94-I-8
C.D.R. Junction	6-12 -109-11W6
C.D.R. Union Zama L.	7-23 -110-12W6
Placid Zama	5- 1 -111- 9W6
B.A. Zama L.	11- 7 -113- 8W6
Hamilton Zama	10-14KR-116- 5W6
Sun et al. Bernadette	8- 1 - 88-25W6
Sun et al. Blueberry	d- 30-K, 94-A-12
Fargo et al. E. Blueberry	a- 22-B, 94-A-13
C.D.R. Union E. Fireweed	d- 55-H, 94-A-13
Altair Sarcee C. & E. Zeke	c- 34-L, 94-A-14
Tex. N.F.A.S. Wargen	a-100-G, 94-H-3
Pure R.O.C. Mike	b- 46-H, 94-H-3
Texcan Donis	d- 55-E, 94-H-2
Union Kcl. R.O.C. Bearberry	d- 71-J, 94-H-2
Union et al. Highland	d- 71-H, 94-H-7
Tenn. C.D.N. S.U.P. Dahl	d- 53-J, 94-H-7
Sinclair Pac. Chinchaga	a- 34-L, 94-H-8
H.B. Union Chinchaga	a- 96-C, 94-H-9
C.D.N. Delhi Foulwater	16-21-101-12W6
C.D.N. Delhi et al. Fontas	7-30-101-11W6
Trend I.O.E. Rainbow S.	15-14-105- 8W6
I.O.E. S. Rainbow	16-24-106- 7W6
H.B.E. Rainbow	16-34-108- 5W6
Shell et al. Rainbow L.	4-34-109- 4W6
Pacific Stoddart	11-10- 86-20W6
White Rose Security Montney	6- 5- 87-18W6
Imp. et al. Rigel	b- 22-K, 94-A-10
Imp. Fina Rigel	6-28- 88-17W6
I.O.E. Fina N. Rigel	d- 57-I, 94-A-10
Amax et al. Lynx	d- 25-A, 94-A-15
Cigol Crush	d- 1-E, 94-A-16
Union H.B. Sinc. Pac. Crush	b- 9-F, 94-A-16
Union H.B. B.A. Ladyfern	d- 48-H, 94-H-1
H.B. Cal. Std. Adskwatin	10-26- 93-13W6
Mobil Chinchaga E.	10-20-100- 7W6
Pure Chinchaga R.	2- 9-100- 6W6
Banff I.O.E. et al. Haigr	14- 5-104- 2W6
C.D.N.-S.U.P. C. & E. Sun Bede	2-29-105- 1W6
Imp. Pac. Parkland	10-28- 81-15W6
Imp. Pac. Argus	16-32- 82-15W6
Imp. Pan Am. Cherry Pt.	6-26- 83-13W6
I.O.E. Pan Am. Boundary	14-21- 84-13W6
Imp. Pac. Boundary	14-17- 85-13W6
Imp. Pan Am. Neptune	6- 8- 85-12W6
I.O.E. Pan Am. Neptune	10- 7- 86-11W6
Pan. Am. Imp. A-1 Clear R.	11-16- 87-11W6
Shell Worsley	6-18- 87- 9W6
H.B. Union B.A. Clear Hills	2- 1- 89- 8W6
Union Notikewin R.	12- 1- 92- 5W6
I.O.E. Lovet	7-32- 94- 4W6
Mob. Shell Hotchkiss	10- 2- 95- 2W6
Shell Botta R.	10-19- 96- 1W6

B. Other Wells Studied

Shell Botta River	10-19-96- 1W6
Mobil Shell Hotchkiss	10- 2- 95- 2W6
Shell Hotchkiss	16-24- 94- 2W6
I.O.E. Lovet	7-32- 94- 4W6
Union Notikewin River	12- 1- 92- 5W6
H.B. Union B.A. Clear Hills	2- 1- 89- 8W6
H.B. Union B.A. Clear Hills	13-15- 89- 9W6
Shell Worsley	6-18- 87- 9W6
Pan Am. Imp. A-1 Clear R.	11-16- 87-11W6
I.O.E. Pan Am. Neptune	10- 7- 86-11W6
Imp. Pan Am. Neptune	6- 8- 85-12W6
Imp. Pac. Boundary	14-17- 85-13W6
I.O.E. Pan Am. Boundary	14-21- 84-13W6
Imp. Pan Am. Cherry Point	6-26- 83-13W6
Imp. Pac. Argus	16-32- 82-15W6
Imp. Pac. Parkland	10-28- 81-15W6
Mobil W. Sahtaneh	c-89-I, 94-I-12
Socony Mobil S. Sierra	a-98-K, 94-I-11
Socony Mobil Sierra	c-78-C, 94-I-14
Kerr McGee et al. Sierra	a-27-F, 94-I-14
S.O.B.C. Calstan Peggo	b-74-A, 94-P-7
Baysel N. Bistcho	12-25-123- 7W6
B.A. North Bistcho	6-13-123-10W6
Roy Am. Cess. Sun Bistcho	1- 4-126- 6W6
Socony Mobil Swat	b-50-F, 94-I-5
Triad Uno-Tex Nogah	c-78-H, 94-I-12
Union et al. Dunvegan	7-13- 81- 5W6
Fina et al. Swat	a-81-A, 94-J-8
Pure Imperial Bull	b-67-J, 94-J-1
Williamson Pacific Bougie	d-31-F, 94-G-15
Pan Am. Beaver River A-3	c-45-K, 94-N-16
B.A. North Bistcho	6-12-123-10W6
H.B. Beatty Lake	A2-16-126- 1W6
Home Chiefco Blucr Bists	6-10-120- 3W6
C.S. et al. Bistcho	10-16-122- 5W6
Dome et al. Bistcho	15-27-122- 5W6
B.A. North Bistcho	11-19-122- 9W6
Mobil et al. Pept.	11-15-123- 1W6
C.S. et al. Bistcho	2-14-122- 7W6
Amax Chevron N. Bistcho	7- 4-123-10W6
Placid et al. East Bistcho	12-25-122- 3W6
Placid et al. East Bistcho	10-20-123- 2W6
Pan Am. B.A. A-1 Thurston	15-23-125- 4W6
Canso et al. Bistcho	9-13-121- 4W6
Skelly Bistcho A #1	5-27-121- 7W6
Canso et al. Bistcho	10- 5-122- 6W6
Pan Am. B.A. A-1 Steen	15-26-120- 4W6
Pan Am. B.A. A-1 Bistcho S.	6- 1-120- 4W6
B.A. Steen River	2-25-120- 5W6
I.O.E. Atlantic Sousa	6-12-122- 5W6
Petcal I.O.E. Basset	16- 3-107- 2W6
Scurry-Rainbow Clear Hills	2-12- 89- 8W6
C.D.N.-S.U.P. C. & E. Zama	4-17-113- 6W6
G.P.D. C.D.N. S.U.P. Osborn	c-63-J, 94-A-13
West Nat. et al. Blueberry	d- 6-D, 94-A-13
Pacific Sinclair Peejay	d-22-H, 94-A-15
Union H.B. Beaverdam	d- 1-L, 94-A-16

Union Hudson's Bay Skwat	b- 69-I, 94-A-16
Imp. Pac. Sirius	d- 21-I, 94-A-14
Pacific West Prod N. Buick	c- 14-F, 94-A-14
Union Aspen	b- 64-K, 94-A-13
Pacific West Prod N. Buick	d- 79-B, 94-A-14
C.D.R. Union Pinto	d- 79-F, 94-A-13
Pacific S.R. Candel N. Peejay	d- 34-I, 94-A-15
Imp. Pan Am. Labiche	b- 55-E, 94-O-13
B.A. Pan Am. Klenteh	c- 15-I, 94-O-6
Pan Am. Philis	a- 65-G, 94-O-16
West Nat. et al. Milo	d- 55-E, 94-J-10
Amerada Shell Cheves	a- 2-D, 94-J-10
West Nat. et al. Evie	d- 64-C, 94-J-15
Frontier et al. Evie	c- 52-I, 94-J-14
Pacific et al. Clarke	d- 99-E, 94-J-9
Frontier et al. Evie	b- 88-H, 94-J-14
Pacific et al. Lum	d- 74-B, 94-J-2
Pacific Fort Nelson	a- 19-G, 94-J-10
Texaco Tsea	b- 99-K, 94-P-5
S.O.B.C. Helmet	b- 49-G, 94-P-7
West Nat. et al. Wildboy	b- 6-A, 94-P-14
Pacific Kathy	c- 52-E, 94-P-3
Atlantic Pacific North Kotcho	c- 22-F, 94-P-3
Texaco N.F.A. S. Tsea	b- 87-F, 94-P-5
C.D.N. S.U.P. et al. Nig	d- 53-J, 94-A-13
Sinclair et al. Datcin	d- 54-G, 94-I-15
Sinclair Pacific Lichen Creek	d- 31-A, 94-I-14
Placid Frontier Gunnel	c- 98-L, 94-I-12
Dome Provo Cego Imp. Sentinel	a- 11-L, 94-I-6
Sinclair et al. Datcin	b- 46-G, 94-I-15
Atlantic Kyklo	d- 48-H, 94-I-11
Imperial Kyklo	b- 73-F, 94-I-11
West Nat. Yoyo	b- 98-E, 94-I-14
Pan Am. I.O.E. A-1 Bearskin	d- 86-F, 94-I-1
Dome et al. Junior	a- 45-E, 94-I-11
Uno-Tex et al. Yoyo	c- 34-I, 94-I-13
I.O.E. Junior	c- 60-E, 94-I-11
Atlantic Tees	c- 15-J, 94-I-6
Forest S.R.C. I.O.E. Cedar	d-100-G, 94-I-2
Pacific et al. Bivouac	c- 68-I, 94-I-1
Banff Aquit Chasm	d- 44-J, 94-I-1
Imp. Fontas	d- 37-B, 94-I-7
Imp. Junior	c- 98-C, 94-I-11
Amerada Crown C.D. Bingo	5-35 - 82- 3W6
C. & E. Pacific Doe Creek	6-10 - 82-13W6
Samedan Decalta Berwyn	2-36 - 82-25W5
I.O.E. et al. Clear River	10- 5 - 84-11W6
Altair H.B. Josck	7-24 - 82-10W6
C.D.R. Royce	2-12 - 83- 8W6
T.P.C. & O. et al. Clear R.	10-30 - 83-11W6
I.O.E. Peace Grove	10-16 - 84- 5W6
B.A. H.B. Union Worsley	7- 4 - 88- 7W6
Shell Worsley	2-25JU- 87- 7W6
Sun Pan Am. Dixonville	2-16 - 87- 2W6
C.D.R. et al. Dixonville	10-35 - 86- 1W6
T.P.C. & O. et al. Clear River	14-21 - 84-10W6
Amax Coop N. Boundary	6-31 - 86-14W6
Atlantic Warrensville	6-30 - 87- 1W6
Shell Clear Hills	4-15 - 89-12W6

Champ Atlantic Imp. Hines	6-28- 85- 3W6
Imp. Pan Am. Bear Canyon	8-16- 83-12W6
C.D.R. Royce	10-32- 82- 7W6
Pacific et al. Worsley	11-19- 87- 4W6
Sun E. Osborn	6-31- 88-13W6
I.O.E. Pac. Inga	16-26- 87-24W6
Pacific West Prod. Stoddart	11- 7- 86-19W6
Marathon Boundary	6- 5- 86-13W6
Dome et al. Boundary	16-35- 83-15W6
Monsanto I.O.E. Fina Rigel	16-11- 87-17W6
Imperial Pan Am. Floral	10-20- 84-12W6
Cego et al. Peace	11-21- 82-16W6
F.P.C. Kilkerran	11-36- 78-15W6
T.G.S. et al. Moberly	10-15- 82-22W6
B.A. Zama North	2-16-117- 4W6
Tenn. et al. Steen River	6- 4-118- 6W6
Pan. Am. Vardie #A1	9-20-115- 8W6
I.O.E. Vela Zama	10-31-115- 5W6
C.D.N.-S.U.P. C. & E. Zama	4-10-112- 6W6
I.O.E. Comment North Rain	8- 7-111- 7W6
C.D.R. Union North Rainbow	4-21-111- 8W6
H.B. Zama North	4- 1-116- 6W6
I.O.E. Sousa	6-28-111- 4W6
Huber Scurry Pinn Galaxy	4- 2-110- 5W6
C.D.R. Little Hay Rainbow	7-15-112-10W6
Pan Am. B.A. A-1 Fire	8-32-112-11W6
H.B. Zama North	13- 7-116- 4W6
Chevron Amber River	1-12-118- 7W6
Home et al. Chiefco Zama N.	3- 7-118- 4W6
Placid Sousa	6-29-110- 4W6
I.O.E. Galaxy	14- 2-110- 5W6
Placid Texaco Zama	10-25-112- 9W6
Pan Am. B-1 Melvin	6-33-115-15W5
Home Aimx Cego Meander	2-25-113-18W5
I.O.D. I.O.E. Cego Rennie	3-22-111- 4W5
C.S.-Cego Ponton E.	10-17-112-12W5
C.D.N.-S.U.P. Dome Provo Zama N.	14-17-118- 4W6
Imp. I.O.E. Capella	6- 5-111- 5W6
Pac. Pan Am. Dome N. Beg	d-37-D, 94-G-8
B.A. Zama Lake	10-22-113- 9W6
C.D.N.-S.U.P. et al. Zama N.	10-14-119- 5W6
Dome et al. Zama	14-31-119- 3W6
B.A. Zama Lake	3- 1-116- 8W6
Banff Mobil Rainbow West	2-18-110- 8W6
Baysel et al. Rainbow	2- 8-110- 8W6
Banff Aquit Black Creek	4- 2-110- 9W6
I.O.E. Pan Am. Huber Nova	10- 5-110- 4W6
Cego Sun Cabot Zama	10- 1-117- 5W6
Fina Zama	4- 9-117- 6W6
Mobil Prism Rain	4-13-110- 6W6
Shell Clear Hills	6- 7- 92-12W6
Sun Chevron Jim Creek	2-27- 90- 1W6
P.F.C. Richfield Daiber	c-98-D, 94-B-16
Mobil Rainbow	12-11-109- 6W6
Banff Mobil Rainbow West	11-27-108- 8W6
I.O.E. Rainbow	13-20-107- 9W6
I.O.E. Arch	3-12-107- 8W6
Homestead et al. Rain S.	3-18-107- 7W6
Banff Aquit. Long Lake	6- 3-107- 6W6

Penzl et al. Steen River	3-19-119- 2W6
Placid et al. East Bistcho	12-25-122- 3W6
I.O.E. Sousa	6-28-111- 4W6
Banff Mobil Rain S.	5- 4-108-10W6
Imp. Pac. Boundary	6-17- 84-14W6
Banff Mobil Nonta	7-35-109- 7W6
H.B. Rainbow East	12-16-109- 5W6
Tenneco et al. Spectrum	13-14-108- 6W6
Banff Mobil Kitu	6-23-108- 7W6
Pacific et al. Worsley	7-21- 85- 5W6
Union Hudson's Bay B.A. Foxglove	3-15-A, 94-H-8
Pacific S.R. Can. Del. Falcon	d- 9-C, 94-H-2
Union K.C.L. R.O.C. Yew	d-97-A, 94-H-7
Union H.B. B.A. Cranberry	a-12-D, 94-H-8
Amarillo Drake	d- 5-L, 94-H-1
Altair Sarcee C. & E. N. Zeke	c-20-D, 94-H-3
Pure et al. Donis	b-24-F, 94-H-2
Union H.B. B.A. Aster	a-78-F, 94-H-1
Texaco et al. Nig	a-72-G, 94-H-4
Pacific Nig	b-10-B, 94-H-4
K.C.L. Pure N. Aitken	d-15-E, 94-H-4
Texaco N.F.A. N. Nig	c-63-K, 94-H-4
Monsanto Nig C.R.	b-50-A, 94-H-4
Triad B.P. Birley	c-36-A, 94-H-6
Guyer Mohawk I.O.E. Pyramid	7-22-105- 9W6
Mobil Pan. Am. Rain S.	3-34-106- 8W6
I.O.E. Crescent Rain S.	5-26-106- 9W6
Home Chiefco Blucr Rain S.	7-18-105- 7W6
Mobil South Rainbow	6-14-105- 6W6
Baysel I.O.E. Argus	2-34-104- 8W6
I.O.E. Pyramid	2- 1-106-10W6
Marathon I.O.E. F.P.C. Venus	7-31-102- 9W6
Dome Provo I.O.E. Tartan	15- 7-106- 5W6
B.A. et al. South Rainbow	7-16-106- 6W6
Hudson's Bay-B.A. Boundary	6- 1-100-11W6
T.G.T. K.M. Dickins L. "A"	7-11-124-12W6
West Nat. I.O.E. S. Clarke	d-29-K, 94-J-9
Pacific Tenaka	b- 7-C, 94-J-7
Petcal I.O.E. Keg Post	15- 8-101- 3W6
Mobil Texaco Botha River	6-22- 98- 5W6
White Rose et al. Doig	5-22- 92-10W6
H.B. Shell Clear Prairie	4-32- 91-12W6
Shell Clear Hills	16-17- 90-12W6
Texaco N.F.A. Wolfe	16-17- 88-14W6
Texaco N.F.A. X Boundary	7-15- 87-14W6
Union H.B. Sinc. Pac. Currant	d-37-C, 94-A-16
Kewanee Cigol Melanie	d-68-K, 94-A-9
Pacific West Prod Siphon	6- 4- 87-15W6
Monsanto I.O.E. Fina Rigel	11-19- 87-16W6
Pacific et al. N. Pine	6-27- 85-18W6
Pacific et al. Stoddart	10-35- 85-19W6
Samedan Pacific Haven	9-33- 83-19W6
Sun et al. Blueberry	a-61-L, 94-A-12
Tenn et al. Inga "E"	6-13- 88-24W6
West Nat. et al. Lookout	d-42-J, 94-A-12
Sun et al. Jeans	a-57-A, 94-A-13
C.D.R. Fireweed	3-31-G, 94-A-13
Pure R.O.C. Prepatou	d-99-A, 94-H-3
C.D.R. H.B. Union Chinchaga	c- 2-B, 94-H-9

Pacific Pan. Am. Dome Jedney	b-28-F, 94-G-8
Texaco N.F.A. Warus	b-86-L, 94-I-16
Cego et al. Flatrock	10-27- 84-16W6
I.O.E. et al. Flatrock	5-20- 84-15W6
Imp. Pac. Boundary	16- 9- 85-14W6
Amax Coop N. Boundary	6-31- 87-14W6
Huber et al. Boundary	7- 6- 87-13W6
Pan. Am. I.O.E. B-1 Clear River	10-20- 87-12W6
Shell Clear Hills	10-29- 89-11W6
Shell I.O.E. Notikewin	4-16- 93- 7W6
Mobil Texaco Meikle River	6-13- 96- 4W6
C.D.N.-S.U.P. Whitehall Inga	6- 4- 88-23W6
Tenn A-1 South Inga	16- 7- 87-23W6
Pacific S. Inga	6- 8- 87-23W6
Pacific I.O.E. Cache Creek	13-16- 86-22W6
Apache Pac. W. Stoddart	10-24- 86-21W6
Sun Buick	d-11-C, 94-A-14
Frontier Pembina Wolf	d-14-G, 94-A-15
Medallion Charter Sapphire	b-84-H, 94-A-14
Union Arco Firebird	d-43-D, 94-H-2
Pacific S.R. Candel Weasel	d- 5-B, 94-H-2
Union H.B. Wildmint	d-26-A, 94-H-2
Cigol et al. Snowberry	d-17-D, 94-H-1
Union Hudson's Bay Willow	d-11-G, 94-H-2
Union H.B. Woodrush	b-56-H, 94-H-2
Union Hudson's Bay Alder	c-39-I, 94-H-2
Amarillo Aspen	d-55-E, 94-H-1
Amarillo Groundpine	b-40-K, 94-H-1
Union H.B. B.A. Bogbean	b-72-J, 94-H-1
I.O.E. F.P.C. Venus	10- 2-101- 8W6
T.P.C. & O. Pure Basset Lake	4-26-105- 4W6
I.O.E. Basset	16-22-106- 3W6
Homestead I.O.E. Basset	13-24-108- 1W6
B.A. I.O.E. Negus Creek	4-33-110-24W5
Hudson's Bay Cypress	d-87-C, 94-B-15
Pacific et al. Jedney	d-42-C, 94-G-8
Pacific Imperial N. Bubbles	d-95-B, 94-G-8
Pacific Sunray Imp. Sojer	a-61-L, 94-H-4
Texaco Tepee	d-99-G, 94-G-8
Pacific Imp. Laprise	b-90-C, 94-H-5
Forest S.R.C. I.O.E. Bedji	b-44-I, 94-I-2
C.D.R. West Rainbow	12-10-109-12W6
B.A. Zama Lake	2- 4-114- 7W6
I.O.E. Virgo Zama	8- 8-115- 6W6
B.A. H.B. Zama North	5-30-116- 4W6
Dome Provo Zama N.	10-14-117- 4W6
C.D.N. S.U.P. Dome Zama	10-18-118- 3W6
Penzl et al. Steen River	3-19-119- 2W6
Texaco N.F.A. N. Townsend	a- 8-J, 94-B-9
C.D.R. Union W. Pinto	a-83-E, 94-A-13
West Nat. et al. Aitken	d-30-L, 94-A-13
Tenn Monsanto Nig	d-39-C, 94-H-4
Texaco N.F.A. Nig	c-76-G, 94-H-4
Texaco N.F.A. Nig	c- 6-H, 94-H-4
Imp. Pac. Sunray Wargen	d-33-D, 94-H-6
Imp. Pac. Sunray Wargen	c-58-C, 94-H-6
Texaco N.F.A. Wendy	c-90-G, 94-H-6
Texaco N.F.A. Redeye	a-72-I, 94-H-6
H.B. Union Imp. Paddy	c-14-C, 94-H-16

I.O.E. Beaverskin	c-85-H, 94-I-1
C.D.N.-S.U.P. Fina Sabbath	10-27-106-12W6
Banff Mobil Rain S.	12-27-107-10W6
Banff Mobil Tehze Rain	15-22-108- 9W6
Banff Mobil Rainbow West	9-24-109- 8W6
Imp. I.O.E. Comet	4- 2-110- 7W6
Mobil Hay Lk. Rain	10- 3-111- 6W6
C.D.N.-S.U.P. C. & E. Habay	1-32-113- 5W6
Texcan Fox	d- 7-D, 94-A-16
Union H.B. Moose	d-56-K, 94-A-16
Amax et al. Skwat	a-80-B, 94-H-1
C.D.N.-S.U.P. C. & E. Sun Bede Ck	10-15-106- 1W6
Pacific Shekilie	b-24-A, 94-I-16
Texaco Shekilie River	2- 7-117-10W6
Baysel South Bistcho	3-35-119- 8W6
Mobil et al. Suds Bistcho	13-13-119- 7W6
Canso et al. Bistcho Lake	10-27-119- 6W6
Mobil et al. Turf Bistcho	15-20-121- 6W6
C.S. et al. Bistcho	12-35-121- 5W6
Canso et al. Bistcho Lake	12-20-122- 4W6
Dome et al. Bistcho	10-23-123- 3W6
Placid et al. E. Bistcho	5- 4-124- 2W6
H.B. Beatty Lake	10-28-126- 1W6
Apache Pacific Ft. Nelson	a- 91-C, 94-J-10
Pacific et al. Clarke	c- 54-F, 94-J-10
Pacific et al. Clarke	a-A65-G, 94-J-10
Pacific et al. Clarke	c- 57-J, 94-J-10
Gulf States et al. Fort Nelson	c- 78-I, 94-J-10
Pacific Imp. Clarke	b- 69-L, 94-J-9
Gulf States Imperial	b- 18-D, 94-J-16
Pacific Chuatse	b- 45-H, 94-J-16
C. & E. Sohio Med Kathy	d- 73-H, 94-P-4
Apache Pure Louise	d- 42-I, 94-P-4
Placid Louise	c- 80-L, 94-P-3
S.O.B.C. Calstan Yeka	a- 69-D, 94-P-10
Pan Am. Tenneco A-1 Cordova	b- 34-C, 94-P-16